Two cowpea Rubisco activase isoforms for crop thermotolerance

Armida Gjindali; Rhiannon Page; Catherine J. Ashton; Ingrid Robertson; Mike T. Page; Duncan Bloemers; Peter D. Gould; Dawn Worrall; Douglas J. Orr; Elizabete Carmo-Silva
Lancaster Environment Centre, Lancaster University, Lancaster, LA1 4YQ, UK
Corresponding author email: e.carmosilva@lancaster.ac.uk

Submission date: 31st January 2025
Number of figures: 4 (all figures in colour)
Number of tables: 2
Number of Supporting Information figures: 15 (all figures in colour)
Number of Supporting Information tables: 10
Word count: 9520 (Introduction 1574, M&M 4096, Results 2126, Discussion 1724)

Summary

- A vital crop for sub-Saharan Africa, cowpea productivity is threatened by climate change, including increased heatwave intensity, duration, and frequency. Rubisco activase (Rca) is a key molecular chaperone that maintains Rubisco activity and due to its thermal sensitivity is a key target for improving crop climate resilience.
- We identified and characterised four Rca isoforms in *Vigna unguiculata* (L.) Walp. cv. IT97K-499-35 *in vitro*: Rca1β, Rca8α, Rca10α and Rca10β. Cowpea leaf and plant growth traits were also investigated during a 5-day +10 °C heatwave that included assessment of Rubisco and Rca activity in leaf extracts, and relative changes in the abundance of the four Rca isoforms.
- Cowpea Rca10α and Rca10β had higher thermal maxima, broader thermal optima and higher rates of ATP hydrolysis and Rubisco reactivation *in vitro*. In the absence of water deficit, the heatwave caused only mild effects, including increases in leaf temperature and expression of *Rca10*, small decreases in Rubisco activity and activation state, and unaltered temperature response of Rubisco activation by Rca.
- The superior Rca10α and Rca10β isoforms offer the prospect of enhancing the thermotolerance of cowpea and other crops in anticipation of more extreme future heatwaves.

Keywords: Activase, cowpea, heat stress, photosynthesis, Rca, Rubisco, temperature response, *Vigna unguiculata*.

Introduction

Changes in global temperatures including heatwave events pose significant threats to global food security (Moore *et al.*, 2021), making increased crop resilience against heat stress imperative (Song *et al.*, 2023). Regions closer to the equator, particularly sub-Saharan Africa, are the most vulnerable to rising temperatures (Harboure, 2024). Elevated temperatures can lead to decreased photosynthesis and plant growth (Hatfield & Prueger, 2011; Bagati *et al.*, 2021; Zahra *et al.*, 2023; Becker *et al.*, 2023). Cowpea (*Vigna unguiculata* (L.) Walp) is a major source of protein for populations in sub-Saharan Africa and, despite being adapted to a warm climate, it is still vulnerable to heat stress – even a 1 °C increase in night temperature can result in significant yield loss (Warrag & Hall, 1984; Gonçalves *et al.*, 2016; Mohammed *et al.*, 2024). Therefore, it is imperative to identify physiological and biochemical traits that confer thermotolerance in cowpea to develop heat resilient crops (Barros *et al.*, 2021).

Moderate heat stress, defined as temperatures up to 40 °C (Crafts-Brandner & Salvucci, 2000; Kumar *et al.*, 2009; Ara *et al.*, 2013), has a profound impact on plant photosynthesis, adversely affecting both the electron transport chain and the Calvin-Benson-Bassham (CBB) cycle (Chen *et al.*, 2022). Rubisco and chlorophyll leaf content also decline under moderate heat stress (Mathur *et al.*, 2014). Chlorophyll biosynthesis enzymes exhibit susceptibility to heat stress; however, the reduction in Rubisco content cannot be attributed to denaturation of Rubisco, as alterations in secondary structure are observed only at temperatures exceeding 45 °C (Li *et al.*, 2002; Mathur *et al.*, 2014). Increased temperatures enhance Rubisco carboxylation activity; but also lead to reduced Rubisco specificity and increased O_2 diffusion, both of which result in higher oxygenation over carboxylation and increased photorespiration (Hermida-Carrera *et al.*, 2016; Galmés *et al.*, 2016). Importantly, photorespiration does not fully account for the decline in carbon assimilation during moderate heat stress, as the Rubisco activation state has been demonstrated to decrease under both photorespiratory and non-photorespiratory conditions during mild heat stress (Feller *et al.*, 1998; Crafts-Brandner & Law, 2000; Galmés *et al.*, 2016).

Numerous studies have demonstrated that Rubisco inactivation is one of the primary causes of reduced photosynthetic efficiency during moderate heat stress (Feller *et al.*, 1998; Crafts-Brandner & Law, 2000; Portis, 2003; Ristic *et al.*, 2009; Carmo-Silva *et al.*, 2015; Perdomo *et al.*, 2017; Wijewardene *et al.*, 2021; Scafaro *et al.*, 2023). To catalyse carboxylation or oxygenation, Rubisco catalytic sites require binding of CO_2 and Mg^{2+} as cofactors to form the active carbamylated Rubisco prior to binding the substrate ribulose 1,5-biphosphate (RuBP). Rubisco can become inactivated by the binding of inhibitory sugar phosphates to carbamylated catalytic sites or by misfire products that cannot dissociate and maintain

catalytic sites in their closed, inactive conformation (Orr *et al.*, 2023). Inactivation can also occur when RuBP binds to an uncarbamylated Rubisco catalytic site. Inhibited Rubisco requires its molecular chaperone Rubisco activase (Rca) to restore its activity (Carmo-Silva & Salvucci, 2013). Rca is a nuclear encoded protein that belongs to the AAA+ ATPases superfamily (Hazra *et al.*, 2015) and, in its active multimeric form, exhibits two activities: ATP hydrolysis and Rubisco reactivation (Bhat *et al.*, 2017; Serban *et al.*, 2018). Rca docks on Rubisco's large subunit and, using ATP, performs conformational remodelling to release the inhibitory compound, thus modulating Rubisco activity by facilitating the dissociation of bound inhibitors. Elevated temperatures increase the frequency of Rubisco inactivation due to higher concentrations of some inhibitory substrates (Salvucci & Crafts-Brandner, 2004, p. 20). Furthermore, although Rubisco is a relatively thermostable enzyme, Rca is thermolabile and even a moderate increase in temperature results in loss of its activity (Crafts-Brandner & Salvucci, 2000; Salvucci *et al.*, 2001).

Rca isoforms within a single species vary in their regulatory properties (Zhang & Portis, 1999; Carmo-Silva & Salvucci, 2013; Perdomo *et al.*, 2019; Scafaro *et al.*, 2019b). Many species express two types of Rca isoforms: longer α isoforms (43-47 kDa) and shorter β isoforms (41-43 kDa) that can be encoded either by individual genes or the same gene via alternative splicing (Carmo-Silva *et al.*, 2015). Rca α isoforms contain a C-terminal extension with two cysteine residues shown to form a disulfide bond which is regulated by thioredoxin-f in *Arabidopsis* (Zhang & Portis, 1999). This regulatory mechanism links Rubisco activity with alterations in the redox potential induced by environmental stimuli, such as high light (Zhang *et al.*, 2002; Perdomo *et al.*, 2021). The redox regulation is species-specific, with Solanaceae species such as tobacco (*Nicotiana tabacum* L.) and tomato (*Solanum lycopersicum* L.) containing only the β Rca isoform that lacks the cysteine residues and the redox regulation of the enzyme (Carmo-Silva & Salvucci, 2013). In species containing only redox insensitive Rca, light regulation appears to be mediated by changes in the ADP/ATP ratio of the chloroplast (Carmo-Silva & Salvucci, 2013).

In addition to variation in the number of genes and the isoforms they produce, the expression and relative abundance of Rca isoforms vary among species and as a response to temperature (Law & Crafts-Brandner, 2001; Wang *et al.*, 2010; Degen *et al.*, 2020; Perdomo *et al.*, 2021). In rice (*Oryza sativa* L.) two Rca isoforms are produced via alternative splicing and while Rca β is more abundant under optimal steady state conditions (Wang *et al.*, 2010), heat stress induces upregulation of Rca α (Scafaro *et al.*, 2016). In maize (*Zea mays* L.) the two isoforms derive from two genes *ZmRcaα* and *ZmRcaβ* encoding an α (43 kDa) and a β (41 kDa) isoform respectively (Yin *et al.*, 2014). Under optimal temperature conditions, the ZmRca β protein isoform is expressed in higher levels

108 than ZmRca α and both exhibit comparable diurnal variation in expression levels (Ristic *et*
109 *al.*, 2009). Jiménez *et al*. reported an increase in ZmRca α in seedlings exposed to higher
110 temperatures, however in more mature heat-treated plants this effect was not consistent
111 (Ristic *et al.*, 2009; Stainbrook *et al.*, 2024). In wheat (*Triticum aestivum* L.) there are two
112 *Rca* genes, one of which produces a β isoform while the other (*TaRca2*) is alternatively
113 spliced and produces both an α and a β isoform (Nagarajan & Gill, 2018). The Rca α/β ratio
114 changes when wheat is exposed to heat stress, suggesting that the relative abundance of
115 the different Rca isoforms is linked with the physiological response to heat stress (Warrag &
116 Hall, 1984; Crafts-Brandner & Salvucci, 2000). By contrast, in *Arabidopsis* the Rca isoform
117 ratio is not impacted by heat, with the α and β isoforms originating from alternative splicing
118 continuing to be expressed at a 1:1 ratio (Zhang & Portis, 1999). These species-specific
119 responses of Rca and Rubisco regulation to heat stress illustrate the need to investigate this
120 system directly in the crop of interest.

121 While the exact mechanism of Rca deactivation at high temperatures is still not fully
122 understood, it is evident that the optimum temperature range for Rca is species-specific and
123 in tune with the photosynthetic optimum (Scafaro *et al.*, 2016). Therefore, the temperature at
124 which Rca loses its activity depends on environmental acclimation; i.e., plants that grow at
125 high temperatures, such as cotton and agave, maintain Rca activity at higher temperatures
126 (Salvucci & Crafts-Brandner, 2004; Carmo-Silva & Salvucci, 2011; Scafaro *et al.*, 2016;
127 Shivhare & Mueller-Cajar, 2017). Rca thermotolerance also differs between closely related
128 species and among the native Rca isoforms within a plant species. The wild rice species
129 *Oryza australiensis* Domin and *Oryza meridionalis* Ng. contain thermostable Rca isoforms
130 that enable sustained high Rubisco activity and photosynthetic rate even at 45 °C (Scafaro
131 *et al.*, 2016, 2018). In rice, spinach and cotton, the α isoform exhibits higher thermostability
132 whereas in wheat, it is one of the two shorter β (TaRca1β) isoforms that is most
133 thermostable (Kurek *et al.*, 2007; Wang *et al.*, 2010; Keown & Pearce, 2014; Degen *et al.*,
134 2020). Increasing the thermostability of Rca is considered one of the most promising
135 strategies for increasing Rubisco activity and enhancing photosynthesis under elevated
136 temperature (Carmo-Silva *et al.*, 2015; Wijewardene *et al.*, 2021).

137 In this study we identified four Rca isoforms in cowpea encoded by three genes: *Rca1*, *Rca8*
138 and *Rca10*, with the latter producing two isoforms via alternative splicing. Characterisation of
139 their ATPase and Rubisco reactivation activities across a range of temperatures *in vitro*
140 revealed that the two Rca10 protein isoforms have higher thermal maxima and broader
141 thermal optima for both activities. We then examined the effect of moderate heat stress
142 during a 5-day heatwave at 38 °C (+10°C compared to control) on the expression and
143 abundance of Rca isoforms and subsequent impacts on Rubisco activation in the leaves of

young cowpea plants. Heat treatment resulted in decreased Rubisco activation state and upregulation of *Rca8a* and *Rca10*, however *Rca10* levels were consistently the lowest. Despite upregulation of the more thermotolerant isoforms, the temperature profile of Rubisco reactivation by Rca in leaf extracts remained unaltered in heat-treated plants. Leaf temperature increased by 6 °C during the heatwave, reaching 32 °C, which is within the temperature range where Rca activity is maintained above 70% of the maximum (T_{opt}) for all isoforms. We therefore conclude that warm-adapted cowpea plants can cope with the mild heat stress induced by a 5-day heatwave at 38 °C in the absence of water deficit, which did not impair Rca function. Overexpression of the most thermotolerant, yet least abundant, Rca isoforms in cowpea will enable adaptation to leaf temperatures resulting from heatwaves that are more intense or accompanied by water deficit, which are likely to occur in sub-Saharan Africa.

156 # Materials and Methods

157 ## Gene identification

158 Cowpea *Rca* genes were identified by searching the cowpea genome (Phytozome 12,
159 cowpea genome v1.1) using keywords and known Rca protein sequences from *Arabidopsis*
160 *thaliana*, *Nicotiana tabacum*, and *Triticum aestivum* (Supporting Information Table
161 S1)(Goodstein *et al.*, 2012; Lonardi *et al.*, 2019). This identified 3 genes for *Rca* in cowpea:
162 *Vigun01g219300* (*Rca1*), *Vigun08g150700* (*Rca8*), and *Vigun10g051600* (*Rca10*).
163 Alignment with known sequences and key conserved features of canonical Rcas allowed
164 identification of the products of each gene. Transit peptide sequences for each protein were
165 identified by alignment to known Rca sequences (with known transit peptide locations). The
166 analysis was repeated using the updated Phytozome 13 cowpea genome v1.2 and yielded
167 identical Rca isoforms (Supporting Information Fig.S1). Analysis of transcript sequences
168 showed that *Rca1* encodes a 384 amino acid (aa) mature protein consistent with a β
169 isoform. *Rca8* encodes a 419 aa α isoform and a 295 aa isoform that is shorter than a
170 regular β isoform and unlikely to be functional. *Rca10* encodes both a 419 aa α and a 382 aa
171 β isoform by alternative splicing.

172 The cowpea *HSP20* (*Vigun06g052200*) gene, used as a heat stress marker, was identified
173 as a homolog of the soybean *HSP20* (*Glyma.18g094600*) shown to be upregulated in two
174 soybean cultivars exposed to heat stress (Song *et al.*, 2017). The Arabidopsis homolog
175 (*At4G27670*) is also upregulated in heat stress (eFP Browser Stress Series,
176 https://bar.utoronto.ca/)(Kilian *et al.*, 2007; Winter *et al.*, 2007). The *Glyma.18g094600*
177 coding sequence was downloaded from SoyBase (https://legacy.soybase.org) and used to
178 search the cowpea genome as above (Brown *et al.*, 2021).

179 ## Cloning of cowpea Rca and construction of *E. coli* expression vectors

180 Coding regions for the mature proteins of cowpea Rca1β, Rca8α, Rca10α and Rca10β were
181 codon optimised for *E. coli, de novo* synthesised and subcloned into pUC57 (Kan^R) by Aruru
182 Molecular Ltd. (Dundee, UK). A Golden Gate compatible *E.coli* expression vector was
183 created from the pET His TEV LIC plasmid (a gift from Scott Gradia, Addgene plasmid
184 #29653; http://n2t.net/addgene:29653; RRID:Addgene_29653). Ligation independent cloning
185 was used to add a Golden Gate cassette taken from pICH47742 (part of the MoClo Toolkit
186 that was a gift from Sylvestre Marillonnet, Addgene kit # 1000000044) into pET His TEV LIC,
187 generating the new Golden Gate compatible pET His TEV GG plasmid (Weber *et al.*, 2011;
188 Werner *et al.*, 2012). Cloning a coding region into this vector allows production of a target
189 protein fused to an N-terminal histidine (His) tag that can be removed with TEV protease.
190 PCR was used to add Golden Gate overhangs to the four optimised *Rca* sequences (see

191 Supporting Information Table S2 for primers used). Golden Gate reactions (final volume 15
192 µL) were performed with a 2:1 molar ratio of insert:plasmid and the following reagents (final
193 concentration): 1× T4 DNA Ligase buffer, 0.1 mg mL^{-1} BSA, 1 mM ATP, 40 KU/mL T4 DNA
194 Ligase, 2 KU/mL *Bsa* I. All reagents from NEB, except ATP (Promega). Reaction conditions
195 were 30 cycles of [37 °C for 2 min followed by 16 °C for 3 min], 37 °C for 5 min, 80 °C for 10
196 min, and 16 °C for 1 min. 5 µL of the reaction mix was used to transform *E. coli* DH5α cells.
197 Resulting colonies were used to generate plasmid DNA for sequencing with primers T7F and
198 T7R (Source Bioscience) to verify correct sequence including in-frame fusion of the coding
199 region to the His tag.

200 Recombinant Rca expression and purification

201 Expression constructs were used to transform BL21(DE3)pLysS *E. coli* competent cells
202 (Invitrogen). PCR and sequencing were used to confirm the presence of the correct
203 constructs in the BL21(DE3)plysS *E. coli* cells. Several cell lines were tested for each
204 construct to identify the cell strains with the highest expression levels for the target proteins.
205 Expression experiments were then scaled up for protein purification.

206 Starter cultures (10 mL M9ZB medium, containing kanamycin and chloramphenicol, both at
207 50 µg/mL) were inoculated from glycerol stocks and grown overnight at 37 °C with 225 rpm
208 orbital shaking. Dynamite medium (containing kanamycin and chloramphenicol, at 50 µg/mL)
209 was seeded with the overnight starter culture (10 mL starter culture in 1 L Dynamite
210 medium). This culture was grown for 3-4 h at 37 °C with shaking at 220 rpm until OD_{595}=0.6-
211 0.8 and then IPTG (0.5 mM final concentration) added to initiate protein expression. Cultures
212 were then transferred to 24 °C with 220 rpm shaking for 20 h. Cells were pelleted by
213 centrifugation (5,000 × *g*, 4 °C, 20 min), washed with 40 mL buffer (50 mM HEPES pH 7.2,
214 300 mM NaCl, 5 mM $MgCl_2$), transferred to 50 mL screw capped tubes before finally
215 collecting by centrifugation (5,000 × *g*, 4 °C, 20 min). The pellet was flash frozen in liquid
216 nitrogen and stored at -80 °C.

217 Cell pellets were thawed on ice and resuspended in Lysis Buffer (50 mM HEPES pH 7.2, 5
218 mM $MgCl_2$, 300 mM NaCl, 50 mM Imidazole, 0.1% Triton X-100 (v/v), 10 µM leupeptin, 1
219 mM PMSF), using 7 mL buffer for every 1 g of pellet. Cells were lysed on ice using a probe
220 sonicator and 5 cycles of 30 s on 30 s off until the solution was homogeneous. Cell debris
221 was removed by centrifugation (23,000 × *g*, 4 °C, 30 min) and the soluble fraction pushed
222 through a 0.45 µm syringe filter prior to chromatography.

223 Purification of the Rca protein was achieved using an NGC chromatography system (Bio-
224 Rad, UK), equipped with a nickel-charged IMAC column (1 mL HisTrap Fast Flow, Cytiva)
225 and a desalting column (10 mL Bio-Scale Mini Bio-Gel P6 Desalting Cartridge, Bio-Rad).

226 IMAC and desalting columns were equilibrated with Equilibration Buffer (5 mL: 50 mM
227 HEPES pH 8, 300 mM NaCl, 5 mM $MgCl_2$, 50 mM imidazole) and Final Buffer (13 mL: 50
228 mM HEPES pH 8, 5 mM NaCl, 5% glycerol), respectively. The sample was applied to the
229 IMAC column, followed by Wash Buffer (15 mL: 50 mM HEPES pH 8, 300 mM NaCl, 5 mM
230 $MgCl_2$, 125 mM imidazole). Bound protein was eluted using a higher concentration of
231 imidazole (2.1 mL: 50 mM HEPES pH 8, 300 mM NaCl, 5 mM $MgCl_2$, 300 mM imidazole)
232 and directly applied to the desalting column. Buffer was exchanged with 15 mL Final Buffer
233 and 1 mL fractions collected. Fractions containing protein were identified using a UV/Vis
234 detector reading at 280 nm. Fractions containing the highest protein concentration
235 (determined using Bradford reagent, BIO-RAD) were pooled, ATP and DTT (2 mM and 5
236 mM final concentration respectively) added and 50-100 µL aliquots frozen in liquid nitrogen
237 before storage at -80 °C.

238 *In vitro* characterization of Rca thermal optima

239 The rate of ATP hydrolysis by Rca isoforms was assayed using the method described by
240 Chifflet *et al.* (1988), with modifications as described within Degen *et al.* (2020). ATP
241 hydrolysis was measured at a range of temperatures (20-55 °C) using 5-minute assays, with
242 reactions initiated through addition of Rca (final concentration 1 µM Rca monomer) and
243 quenched via addition of SDS. After quenching, all reactions and standards were kept at 4
244 °C until inorganic phosphate (P_i) determination. The P_i released during ATP hydrolysis was
245 determined by measuring the absorbance of molybdenum blue at 850 nm in a
246 spectrophotometer (SpectroStar Nano, BMG Labtech, UK).

247 Rubisco reactivation assays were conducted at a range of temperatures (20-45 °C) following
248 the procedures of Barta *et al.* (2011) and Degen *et al.* (2020). Briefly, Rubisco purified as per
249 Amaral *et al.* (2024) was used to prepare inhibited Rubisco complexes (ER) through
250 incubation with RuBP overnight at 4 °C. The two-stage reactivation assay comprises a first
251 stage assay where Rca is added to inhibited Rubisco (ER) at a test temperature (20-45 °C),
252 with aliquots from this assay taken at time intervals to initiate the second stage assay that
253 measures Rubisco activity. This Rubisco activity is a function of the Rca, time allowed for
254 reactivation, and the temperature of the first stage (Supporting Information Fig. S2). With
255 known quantities of Rca and Rubisco, and appropriate controls as detailed within Degen *et*
256 *al.* (2020), Rca reactivation of Rubisco can be established. Maximum Rubisco activity was
257 determined at every temperature and was comparable among assays with each of the four
258 Rca isoforms.

259 Independent purifications of each isoform were used as biological replicates. For ATPase
260 activity, three biological replicates were measured for Rca8α and four for the each of the rest

261 of the isoforms. For Rubisco reactivation, four biological replicates were measured for
262 temperatures 20-32 °C and three for temperatures 38-45 °C. To estimate maximum ATP
263 hydrolysis and Rubisco activation activities and the corresponding temperatures at which the
264 maximum values are attained, second- to third-order polynomials and generalized additive
265 models (GAM) were fitted to the experimental data using the gam function from the mgcv
266 1.8–24 package in R (Wood, 2017). The model that best fit the experimental data was
267 selected based on the Akaike information criterion using the AIC function (Akaike, 1974)
268 (Supporting Information Table S4). The selected model was fitted to each set of the
269 biological replicates (Table 1) as well as the whole dataset (Supporting Information Table
270 S3). T_{max} was calculated as the temperature corresponding to maximum activity. T_{opt} was
271 calculated as the range where activity was maintained above 70% of maximum value. $T_{0.5}$
272 was calculated as the temperature where activity dropped below 50% of maximum value.

273 Plant growth and sampling

274 *Vigna unguiculata* (L.) Walp. cv. IT97K-499-35 seeds (kindly provided by B.B. Singh) were
275 germinated in 0.6 L Deepots (D40H, Stuewe & Sons) containing 1:1 (v:v) mixture of nutrient-
276 rich compost (Petersfield Growing Mediums) and silver sand (horticultural grade, Royal
277 Horticultural Society). Plants were grown in eight growth cabinets (MC1000, Snijders Labs)
278 and watered as needed to soil saturation. Cabinets were maintained at day/night
279 temperatures of 28/18 °C, 70% relative humidity and 400 ppm CO_2 concentration (control
280 conditions). A 12 h photoperiod of constant light of 850 μmol m^{-2} s^{-1} at canopy level was
281 maintained via LED lighting (NS1 spectrum, Valoya). Four cabinets were randomly selected
282 to apply a heat treatment starting at 13 days after sowing (das) including an intermediate day
283 with day/night temperatures of 34/24 °C followed by 5 days of 38/28 °C (Supporting
284 Information Fig. S3a). Data loggers (OM-EL_USB-2, Omega Engineering Ltd.) were placed
285 at canopy level in each cabinet to record temperature and relative humidity every 15 minutes
286 (Supporting Information Fig. S3b).

287 Twenty cowpea plants were grown in each cabinet and sampled or measured for different
288 analyses following a randomised design (Supporting Information Fig. S4). All samples and
289 measurements were taken from the central leaflet of the first trifoliate leaf. Leaf disc samples
290 were taken 4-5 h into the light period, after which plants were cut above the unifoliate leaves
291 to reduce shading of neighbouring plants. Separate plants were used for sample collection in
292 subsequent time points. For non-destructive measurements, such as plant growth traits and
293 chlorophyll content, the same individuals were measured at all time points.

294 Growth measurements were obtained at 15, 17 and 22 das (days 2 and 4 of the heatwave
295 and on day 4 of the post-heatwave recovery period, Supporting Information Fig. S6). Leaf

296 chlorophyll content was estimated using a chlorophyll concentration meter (MC-100,
297 Apogee) by measuring 3 positions on the central leaflet for each plant. Plant height was
298 measured using a ruler from the soil level to the apical meristem. Leaf length and width
299 (widest part perpendicular to the length) were also measured with a ruler for the central
300 leaflet only. Leaf thickness was measured with a digitronic calliper 110-DBL (Moore &
301 Wright). Total above-ground biomass was determined on a separate set of plants by drying
302 leaves and stems at 60 °C until constant weight.

303 Chlorophyll fluorescence (method below) measurements were conducted every day of the
304 heatwave. Three 0.38 cm^2 leaf discs were excised and quickly placed with the adaxial
305 surface upwards on a single layer of wet filter paper on a thin plastic tray (<0.5 mm) and
306 immediately transported to the fluorescence imager.

307 A thermal imaging camera (CAT S60 smartphone, Caterpillar) was used prior to sampling to
308 assess T_{leaf}. Each image was later analysed with FLIR Thermal Studio software (Teledyne
309 FLIR LLC), providing the mean temperature across an area of the leaf surface (Supporting
310 Information Fig. S5).

311 For RNA-seq analyses (method below), four 0.55 cm^2 leaf discs were collected from 4
312 independent biological replicates per treatment per timepoint (days 1, 3 and 5 of heatwave)
313 using a cork borer, then immediately snap frozen in liquid nitrogen and stored at -80 °C.

314 For protein and Rubisco analyses, four 0.55 cm^2 leaf discs were excised as above and
315 quickly placed with the adaxial surface upwards on a single layer of wet filter paper to
316 maintain turgidity. The filter paper was contained in a thin plastic tray and positioned on the
317 surface of the water in a circulating water bath in the artificial sunlight simulation rig (Taylor
318 *et al.*, 2022). PPFD at leaf-disc-level was 850 µmol m^{-2} s^{-1}. Water bath temperature was
319 maintained at 26 °C or 32 °C (±0.1 °C) for control or heat-treated plants, respectively, to
320 mimic leaf temperatures in the growth cabinet. After 1 h incubation leaf discs were quickly
321 blotted on absorbent paper to remove excess moisture, then immediately frozen in liquid
322 nitrogen and stored at -80 °C.

323 For Rubisco reactivation in leaf extracts (LE), eight 0.55 cm^2 leaf discs were sampled on day
324 5 of the heatwave. A different plant was used for each of the seven temperatures of the
325 temperature response curve (20, 25, 32, 38, 40, 45 °C). Samples were quickly frozen in
326 liquid nitrogen, then stored at -80 °C until further analysis.

327 Chlorophyll fluorescence

328 Samples were analysed using a chlorophyll fluorescence imager (closed 800C FluorCam,
329 Photon System Instruments). The imager contained a customized temperature-controlled

330 sample surface area which comprised an aluminium plate with imbedded copper piping
331 connected to a circulating temperature-controlled water bath (Optima TX150, Grant
332 Instruments). The filter paper was in contact with sponges which acted as water reservoirs to
333 ensure the paper remained wet during analysis (Supporting Information Fig. S7a). The
334 temperature of the sample surface area and leaf discs were recorded using type k
335 thermocouples and a data logger (RDXL4SD, Omega). Additional thermocouple wires were
336 placed in contact with the sample surface area, and extra leaf discs, to record temperature
337 throughout the analysis (Supporting Information Fig. S7a). Samples were first dark adapted
338 for 1 h at 26 °C. After dark adaptation, the Fv/Fm protocol in the software (FluorCam 7,
339 Photon System Instruments) was used to make measurements of the maximum quantum
340 efficiency of photosystem II over a range of temperatures. The temperature of the leaf discs
341 was used to assess when the measurement temperature had been reached and was stable.
342 Once stable, the temperature was held for 3 min before the Fv/Fm measurement was
343 taken.

344 The data for each set of three leaf discs from the same plant were averaged and plateauing
345 Fv/Fm points at higher temperatures were removed before the remaining data were used to
346 calculate T_{crit} (Supporting Information Fig. S7b) with the segmented function from the
347 segmented package(Muggeo, 2017) in R. This function uses a previously fitted linear model
348 to identify a breakpoint and fits two linear models before and after the breakpoint. The
349 breakpoint in the Fv/Fm curve was taken as T_{crit} while the slopes of the two linear models
350 were taken as m1 & m2 (Supporting Information Fig. S7b, c, d).

351 Protein extraction, Rubisco activity and content

352 Proteins were extracted from leaf disc samples and Rubisco activity assays were performed
353 in a randomised order, as described previously (Taylor *et al.*, 2022; Ashton *et al.*, 2024). The
354 activation state of Rubisco was calculated as the ratio of initial to total activity. In short,
355 aliquots of the leaf extract supernatant were added to an assay mix containing $^{14}CO_2$ and
356 RuBP to initiate assays that gave an estimate of Rubisco initial activity, whereas Rubisco
357 total activity was measured after allowing a 3-minute incubation period of the leaf extract in
358 the assay mix without RuBP to allow full carbamylation of Rubisco.

359 Aliquots of leaf extract supernatant were also used for determining Rubisco content via ^{14}C-
360 CABP (2-carboxy-D-arabinitol 1,5-bisphosphate) binding, as previously described (Ruuska
361 *et al.*, 1998; Ashton *et al.*, 2024) and total soluble protein content, using the Bradford method
362 (Bradford, 1976).

363 ## Gene expressions analysis

364 Frozen leaf disc samples were ground to a fine powder in liquid nitrogen using a pestle and
365 mortar. Total RNA was extracted from 20-30 mg tissue using a NucleoSpin™ RNA Plant Kit
366 (Macherey-Nagel) including a DNase treatment, according to the manufacturer's
367 instructions. RNA concentration and quality were determined by spectrophotometry using a
368 microplate reader and LVis plate (SPECTROstar Nano, BMG Labtech) (Supporting
369 Information Table S5). Further QC analysis of RNA samples was performed by Novogene
370 using a Qubit fluorometer (Invitrogen) and an Agilent 5400 fragment analyzer, followed by
371 mRNA purification (using poly-T oligo-attached magnetic beads), library construction and 2 x
372 150 bp paired-end (PE150) sequencing using an Illumina NovaSeq 6000 (read depth of 30
373 million reads).

374 An initial filtering was applied to the raw data to remove reads containing adapters,
375 containing N > 10% (N represents bases that cannot be determined) and low-quality bases
376 (Phred < 5). Further read quality assessment and trimming was performed using the FastQC
377 tool, version 0.12.1 (http://www.bioinformatics.babraham.ac.uk/projects/fastqc/) and
378 cutadapt, version 4.2 (Martin, 2011). Low quality bases (Phred < 30) were trimmed from 3'
379 ends of each read, flanking N bases were removed and trimmed reads shorter than 50 bp
380 were discarded (for sequencing and alignment statistics see Supporting Information Table
381 S6).

382 Cowpea IT97K-499-35 reference transcriptome v1.2 (Lonardi *et al.*, 2019; Liang *et al.*, 2024)
383 was downloaded from Phytozome 13 (Goodstein *et al.*, 2012). Salmon, version 1.10.1 (Patro
384 *et al.*, 2017) was first used to index the reference transcriptome and then quantify expression
385 of clean reads at the transcript level. To identify changes in the cowpea Rca transcripts TPM
386 values were extracted from the Salmon Quant.sf output files for Rca, RbcS and HSP20
387 transcripts. Three transcripts are present for Rca1β (the first two result in the same protein,
388 the third is missing some of the N domain) and TPM values for all three were combined.
389 Three transcripts exist for Rca8α (transcripts 2 and 3 are non-functional and have low
390 expression) so here we only present data for the first transcript. For Rca10 transcripts 1, 3
391 and 4 are combined to give total expression for the alpha isoform and transcript 2 alone
392 represents the beta isoform. The three transcripts for RbcS were also combined.

393 Global gene expression analysis was carried out in R version 4.4.1 (2024-06-14, Race for
394 Your Life). Raw counts from Salmon were loaded into EdgeR 4.2.1 using tximport 1.32.0 and
395 rtracklayer 1.64.0. Transcript data for each gene was combined at this stage so that all
396 global analysis was performed at the gene-level. PCA plot was made using logCPM the
397 PCAtools 2.16.0 to check that biological replicates group together and to look for outlying

398 samples. Here we used the counts per million (CPM) to remove the variability due to library
399 depth. The EdgeR trimmed mean of M-values (TMM) method was used for normalisation of
400 read counts. The data was filtered using a CPM threshold to remove genes with zero or near
401 zero expression. A generalised linear model was then fitted to the normalised and filtered
402 data for each gene. Empirical Bayes quasi-likelihood F-tests were used to test whether
403 genes were significantly differentially expressed between heat-treated and control plants on
404 each day of the heatwave. To control for multiple testing, p-values were calculated using the
405 false discovery rate (FDR) of Benjamini-Hochberg. Differentially expressed genes (DEGs)
406 were then identified using the threshold values of a false discovery rate (FDR) of < 0.05 and
407 a log2 (|fold change|) of >1.5.

408 Rca gene expression changes were validated via RT-qPCR (Supporting Information Fig.
409 S11). For sampling and detailed methodology see Supporting Information Tables S7 & 8.

410 Rca quantification via western blotting

411 To quantify the abundance of different Rca protein isoforms, an aliquot of supernatant
412 resulting from Rubisco analysis was mixed with SDS-PAGE loading buffer and separated as
413 previously described on Perdomo *et al.* (2018) on a 12% TGX Stain-Free gel (Bio-Rad). Gels
414 were imaged to assess total protein before transfer to a nitrocellulose membrane using a dry
415 blotting system (iBlot2, Thermo Fisher Scientific). Membranes were stained with REVERT
416 Total Protein Stain for normalisation (Li-Cor Biosciences) and imaged prior to application of
417 antibodies. To compare the abundance of α and β isoforms of Rca, an antibody with broad
418 specificity for both isoforms was used (Feller *et al.*, 1998,a gift from Michael Salvucci), with
419 detection via a secondary fluor-tagged antibody (IRDye800CW, Li-Cor Biosciences,
420 RRID:AB_1660973). A dilution series of a pooled sample was run on every gel alongside the
421 samples to verify antibody detection was within the linear range. To quantify Rca8α, a more
422 specific antibody was used (Abcalis) in place of the broad specificity antibody. The anti-
423 Rca8α specific antibody was generated using phage display with the peptide selected
424 targeted against KRGAFYGKAAQQINVP (amino acid residue 376-391), as described in
425 Bloemers & Carmo-Silva (2024). All blot images were obtained using an Odyssey FC (Li-Cor
426 Biosciences). Empiria studio software (version 2.3.0.154, Li-Cor Biosciences) was used for
427 image data analysis and normalisation with the total protein stain, with values determined as
428 signal intensity.

429 Characterization of Rca thermal optima in leaf extracts

430 Rubisco reactivation by Rca in leaf extracts was determined as described in Carmo-Silva &
431 Salvucci (2011). Eight leaf discs per plant were sampled from the youngest fully expanded
432 leaf on day 5 of the heatwave. Separate samples were used for assaying each of the seven

433 temperatures of the temperature response curve shown in Figure 4, and eight plant sample
434 replicates were used per temperature. Samples were stored at -80 °C until further analysis.
435 One replicate of samples from one cabinet at control and one cabinet at high temperature
436 was used in each day of Rca assays, with samples allocated randomly to each assay
437 temperature. Supporting Information Fig. S14 illustrates the method which uses leaf extracts
438 as the source of both Rubisco and Rca, incubates sub-aliquots with different assays mixes,
439 and then carries out a two-stage assay very similar to the assay with the purified proteins.
440 This enables determination of the capacity of a population of Rca, drawn from plants grown
441 in different conditions, to reactivate Rubisco. Model fitting and temperature parameter (T_{max},
442 T_{opt} and $T_{0.5}$) calculations were conducted as described for the *in vitro* Rca activity assays
443 above. From the same samples, aliquots of leaf homogenate were used for leaf chlorophyll
444 content determination as described previously in Sales *et al.* (2022) and Taylor *et al.* (2020),
445 according to equations by Lichtenthaler (1987). Aliquots of the desalted extract were used
446 for total soluble protein (TSP) content determination using the Bradford method (Bradford,
447 1976). Results are presented in Supporting Information Table S3.

448 Data analyses

449 Geneious 2024.0.7 was used to generate protein alignments depicted in Figure 1a. Data
450 was processed using R 4.3.1 and RStudio 2024.09.0. Graphs were prepared using the
451 ggplot 2 (Wickham, 2017), EnhancedVolcano (Blighe *et al.*, 2018), VennDiagramm (Chen,
452 2022), ggpubr (Kassambara, 2023) and patchwork (Lin Pedersen, 2024) R packages.
453 Outliers were detected with the Outliers package using Tukey's fences method, where
454 outliers are defined as extreme values that are 1.5 times the interquartile range (1.5 IQR)
455 below the first quartile or 1.5 IQR above the third quartile. Box plots show medians and the
456 first and third quartiles (25th and 75th percentiles), and whiskers extend from the hinge to the
457 largest or smallest value. Symbols represent individual data points (technical or biological
458 replicates defined for each plot either on methods or figure legend). Bar plots show means
459 and error bars represent standard error. For statistical analysis, normality of data was
460 assessed using the Shapiro-Wilk test and equality of variances using the Levene test. For
461 measurements on multiple days, two-way ANOVA tests were applied to determine if there
462 were significant day, treatment or interactive effects, followed by post-hoc Tukey tests for
463 multiple comparisons with Bonferroni correction. Compact letters display (cld) were
464 generated after the post-hoc pairwise comparisons using packages mutlicomp (Bretz *et al.*,
465 2016) and multicompView (Graves *et al.*, 2024). In cases where there was a slight violation
466 of normality or homogeneity of variance when data between different days was compared,
467 two-way ANOVA was still chosen as the most robust method. If normality and variance were
468 severely violated, data was log transformed, and two-way ANOVA was applied to the

transformed data provided assumptions were not severely violated in the transformed data. For measurements taken at a single timepoint (growth parameters), t-test was used to determine statistical significance between treatments. Statistical analysis results and full datasets are provided in the Source Data file.

Results

Cowpea contains four Rubisco activase isoforms

The cowpea genome contains three genes that encode Rca. The gene on chromosome 1 (*Vigun01g219300)* encodes an Rca β, the gene on chromosome 8 (*Vigun08g150700)* an Rca α, and the gene on chromosome 10 (*Vigun10g051600)* encodes both Rca α and β isoforms via alternative splicing (Figure 1a). The gene on chromosome 8 also encodes a truncated version of Rca, however this would not produce a canonical, fully functional Rca as it has a premature stop codon before the α-helical domain which is necessary for the recognition of Rubisco by Rca (Portis *et al.*, 2008). Rca isoforms in cowpea exhibit minor sequence differences, primarily in the N-terminal region (the flexible domain critical for Rubisco binding) (Stotz *et al.*, 2011; Shivhare *et al.*, 2019, p. 20) and the α-helical domain (Supporting Information Fig. S1). These variations may contribute to functional diversity of Rca in cowpea, potentially allowing for fine-tuning of responses to different environmental conditions.

Cowpea Rca isoforms differ in thermal optima of activity *in vitro*

Previous studies have shown the potential for intraspecies variation of Rca thermal optima (Degen *et al.*, 2020). With four distinct isoforms in cowpea and its known ability to grow in warm (20-37 °C) temperatures (Barros *et al.*, 2021), recombinant versions of each isoform were produced for *in vitro* characterisation of cowpea Rca thermal optima (Figure 1b). Both enzyme activities were assessed, i.e., the ability to reactivate inhibited cowpea Rubisco and the ATPase activity that drives reactivation (Robinson & Portis, 1989). Rubisco reactivation by Rca was calculated after accounting for the spontaneous reactivation of Rubisco, expressed as a percentage of maximum Rubisco activity. The spontaneous reactivation of Rubisco, although insignificant at lower temperatures, increases with temperature (Supporting Information Fig. S2) as the Rubisco catalytic site becomes more flexible. For all the Rca isoforms, the temperature corresponding to the peak of activity (T_{max}), the range of temperatures at which activity was maintained above 70% of the maximum value (T_{opt}) and the temperature at which activity drops below 50% of the maximum ($T_{0.5}$) were consistently higher for ATPase activity than for Rubisco reactivation activity (Table 1). A higher sensitivity of Rubisco reactivation compared to ATP hydrolysis has been previously reported and may be due to the interaction with Rubisco being the key step impacted by elevated temperatures in Rca (Degen *et al.*, 2020). It has also been shown that while ATP hydrolysis can be catalysed by Rca oligomers consisting of three subunits, Rubisco reactivation requires oligomers containing more than three subunits (Keown *et al.*, 2013; Hazra *et al.*, 2015).

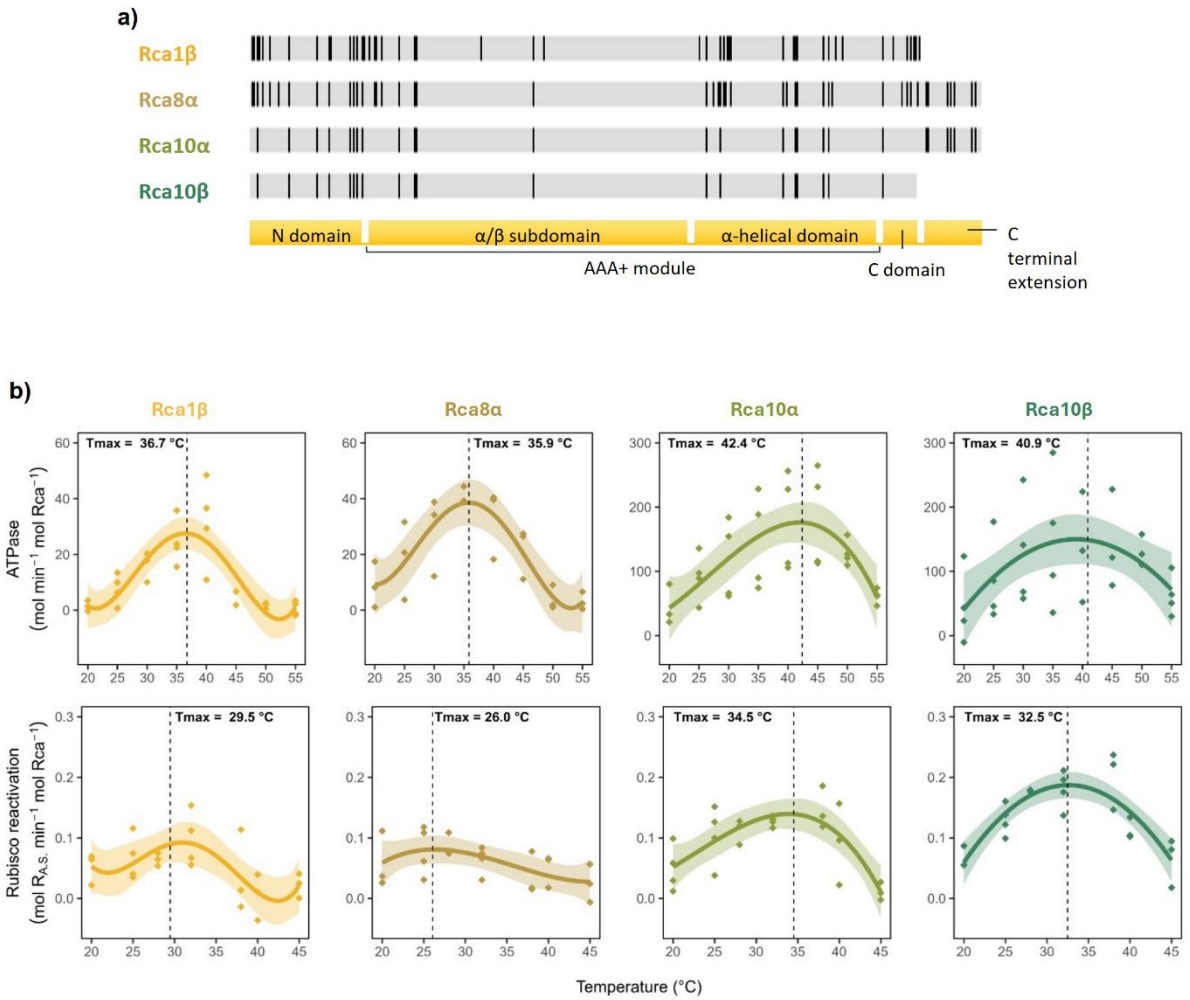

Figure 1. Temperature response of cowpea Rca isoforms in vitro. a) Amino acid residue alignment of the four cowpea Rca isoforms encoded by genes located on chromosomes 1, 8 and 10. Black vertical lines indicate differences in sequence among the genes. The following corresponding regions of the protein are shown: N-domain, α/β subdomain, α-helical domain, C-domain, and C-terminal extension. b) Temperature response of ATP hydrolysis and Rubisco activation by cowpea Rubisco activase isoforms *in vitro*. Rate of ATP hydrolysis and Rubisco reactivation by recombinantly produced purified cowpea Rca isoforms Rca1β, Rca8α, Rca10α and Rca10β. Assays were performed at the indicated temperatures using 1 μM purified Rca and 5 mM ATP. Activation of pre-inhibited Rubisco used 5 μM Rubisco active sites ($R_{A.S.}$) in the ER form (1:5 Rca:$R_{A.S}$). Rubisco activation is presented relative to maximum Rubisco activity, determined as the Rubisco activity when Rca is allowed to reactivate inhibited Rubisco for 5 min. Values represent biological replicates (independent purifications; n=3-4 biological replicates). Lines represent the best fit for each enzyme (selected by the Akaike information criterion) and shaded areas denote the 95% confidence interval for each fit (Supporting Information Table S4). Full sample data are provided in the source data file.

524 **Table 1.Temperature response of *in vitro* Rubisco activase (Rca) activity.** Maximum
525 rate of ATP hydrolysis and Rubisco activation and corresponding temperature (T_{max}),
526 optimum temperature range (T_{opt}, above 70% activity) and temperature above the optimum
527 at which 50% of the maximum activity remains ($T_{0.5}$). Values were estimated from best-fit
528 models that describe the *in vitro* temperature response of each Rca isoform (Supporting
529 Information Table S4). The best-fit model was applied to each of three biological replicates
530 with complete temperature response curves shown in Figure 1b. The first biological replicate
531 was excluded from the fitting of the individual replicates because the temperature response
532 of Rca activity was incomplete (determined only up to 32°C); this replicate is included in the
533 model fitting to the complete temperature response data set (Supporting Information Table
534 S3). Values show here are the mean ± standard error of the mean of values determined for
535 individual replicates of temperature response curves (n=3).

Rca Isoform	$ATPase_{max}$ (mol min^{-1} mol Rca^{-1})	T_{max} (°C)	T_{opt} (°C)	$T_{0.5}$ (°C)
1β	28.0 ± 5.3	36.7 ± 0.5	29.9 – 43.4	43.4 ± 1.1
8α	35.9 ± 8.1	35.9 ± 0.7	28.4 – 43.1	45.6 ± 0.2
10α	179.0 ± 36.8	42.6 ± 1.1	30.9 – 51.6	53.6 ± 0.7
10β	183.4 ± 58.5	40.9 ± 1.1	28.5 – 52.1	53.5 ± 0.3
Rca Isoform	**$Rubisco\ reactivation_{max}$ (mol $R_{A.S.}$ min^{-1} mol Rca^{-1})**	**T_{max} (°C)**	**T_{opt} (°C)**	**$T_{0.5}$ (°C)**
1β	0.10 ± 0.03	29.5 ± 1.2	27.7 – 34.4	36.1 ± 1.5
8α	0.09 ± 0.02	26.0 ± 2.9	22.1 – 36.0	41.0 ± 2.9
10α	0.14 ± 0.01	34.5 ± 1.0	26.5 – 40.8	42.4 ± 0.2
10β	0.19 ± 0.01	32.5 ± 0.4	24.0 – 40.9	43.3 ± 0.8

536

537 The two Rca isoforms encoded by *Rca10* were faster at hydrolysing ATP and reactivating
538 Rubisco, had higher thermal maxima (T_{max}), broader thermal optima (T_{opt}), and showed
539 thermal sensitivity ($T_{0.5}$) at warmer temperatures compared to the other two isoforms (Figure
540 1b;Table 1). T_{max}, T_{opt}, and $T_{0.5}$ calculated for both ATP hydrolysis and Rubisco reactivation
541 were generally similar for Rca1β and Rca 8α (Table 1), but Rca1β exhibited the lowest $T_{0.5}$
542 for reactivation activity (36.1 ± 1.5 °C). Up to 34 °C, all Rca isoforms maintained at least
543 70% of maximum Rubisco reactivation activity. Rca10α exhibited the highest temperature
544 corresponding to the peak of activity for both ATP hydrolysis (T_{max} = 42.6 ± 1.1 °C) and
545 Rubisco reactivation (T_{max} = 34.5 ± 1.0 °C). T_{max} values for Rca10α and Rca10β were at
546 least 3 °C higher for both ATP hydrolysis and Rubisco reactivation relative to Rca1β and
547 Rca8α (Table 1). Combined, the results show that the cowpea Rca10α and Rca10β isoforms
548 have faster rates, higher thermal maxima, broader thermal optima, and are less sensitive to
549 warmer temperatures than Rca1β and Rca8α.

550 A 5-day heatwave of +10 °C causes mild heat stress in cowpea

551 To investigate heat-induced changes in cowpea Rca *in planta*, young plants were exposed
552 to a 5-day heatwave consisting of an increase of 10 °C during both day and night. Plants
553 were cultivated for two weeks at 28/18 °C day/night, then in half of the controlled
554 environment cabinets the temperature was increased to 34/24 °C day/night for one day and
555 subsequently to 38/28 °C day/night for five days (Figure 2a, Supporting Information Fig. S3,
556 4). The intermediate day aimed to resemble a gradual increase in temperature in field
557 conditions. Plants were well watered throughout the heatwave as the focus was on the
558 impact of heat on Rca and we wanted to avoid confounding effects of water deficit on CO_2
559 diffusion and assimilation. Cabinet and leaf temperatures were monitored throughout the
560 experiment to ensure the plants were under heat stress conditions, with heat-treated plants
561 showing a 6 °C increase in leaf temperature to 32 °C (Figure 2a, Supporting Information Fig.
562 S5). Thus, plants experiencing the heatwave had leaf temperatures within the T_{opt} of Rca
563 activity.

564 Plant growth traits were determined four days after the heatwave, after plants were allowed
565 to recover, and showed that the 5-day heatwave of +10 °C had only a mild impact on
566 cowpea (Figure 2b). Exposure to elevated temperature resulted in decreased leaf thickness
567 and increased plant height; however, no effect on aboveground dry biomass was observed.
568 Total chlorophyll also decreased in leaves that had been exposed to heat when determined
569 four days after the heatwave (Figure 2b). Measurement of leaf and plant traits during the
570 heatwave suggested an initial increase in the rate of cowpea leaf and plant growth (day 2,
571 Supporting Information Fig. S6), but only minimal differences between control and heat at
572 the end of and after the heatwave.

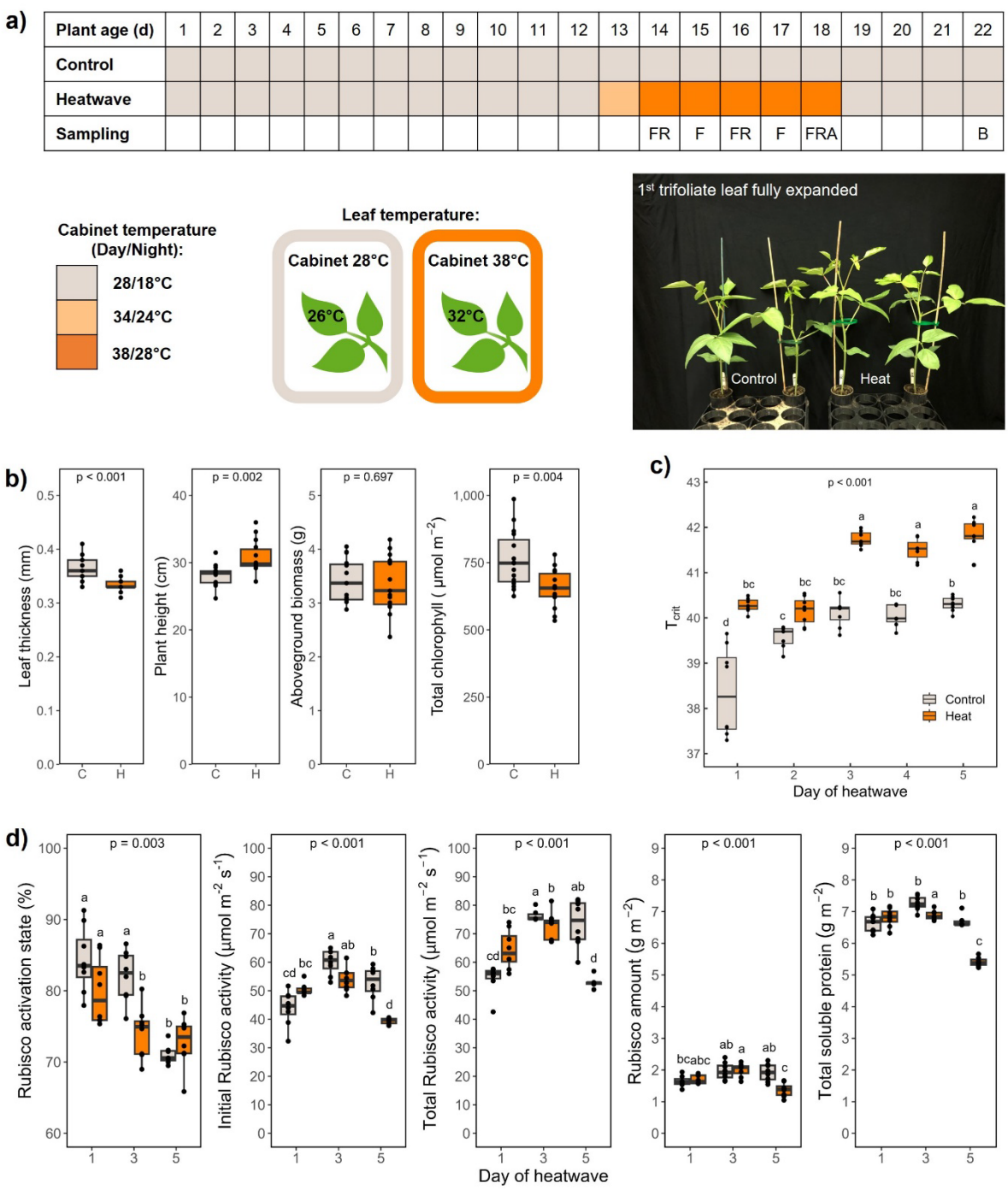

Figure 2. Cowpea response to a heatwave in controlled environment. a) Experimental design, heatwave and sampling times. Plants were grown at 28/18 °C day/night for 13 days, then exposed to an intermediate heat treatment for a day at 34/24 °C day/night before being exposed to a 38/28 °C day/night heatwave for five days. Sampling: (F) photosystem II maximum efficiency (Fv/Fm) was measured daily during the heatwave; (R) leaf discs for RNA-seq analysis, total soluble protein (TSP), Rubisco activity and amount were sampled on days 1, 3 and 5 of the heatwave; (A) samples for Rca temperature response in leaf extracts were taken on day 5 of heatwave; (B) growth parameters and biomass were measured on

day 22 of plant growth, four days after the end of the heatwave. Cabinet and leaf temperature were monitored daily. b) Leaf and whole plant growth parameters were measured four days after the end of the heatwave (n=15). Relative chlorophyll content was determined using a concentration meter based on leaf reflectance. c) T_{crit} was calculated for each day of the heatwave as the breaking point where the two Fv/Fm slopes meet (Supporting Information Fig. S7). d) Rubisco activation state (n=7-8), (b) initial (n=7-8) and (c) total activity per leaf area (n=6-8), Rubisco amount (n=7-8) and total soluble protein (TSP; n=6-8) were measured in leaf extracts on days 1, 3 and 5 of the heatwave. P-values were calculated using two-way ANOVA followed by Tukey post-hoc tests. Full sample data are provided in the source data file.

As a proxy for photosynthetic activity, photosystem II (PSII) maximum efficiency (Fv/Fm) was monitored throughout the heatwave (Supporting Information Fig. S7). Changes in Fv/Fm indicate modifications in the functionality of PSII reaction centres, with a decrease indicating photooxidative damage and reduced photochemistry quantum yield (Murchie & Lawson, 2013). Fv/Fm data collected from plants throughout the heatwave enabled determination of T_{crit} (Figure 2c), which corresponds to the temperature at which chlorophyll *a* fluorescence rises rapidly in response to temperature due to thermal damage in PSII, and is used as an indicator of photosynthetic thermal stability (Perez & Feeley, 2020; Posch *et al.*, 2022). In heat-treated cowpea, Fv/Fm did not decline compared to control plants (Supporting Information Fig. S7e), indicating that no irreversible damage was caused to PSII reaction centres due to heat stress. In fact, heat-treated plants showed a progressive increase in the temperature at which Fv/Fm decreased, resulting in a significantly higher T_{crit} after 3 days, denoting increased PSII thermal stability ($p < 0.001$, Figure 2c). These results indicate a dynamic response that allows for PSII efficiency to adapt to warmer conditions.

Heat stress induces a decline in Rubisco activation state

In contrast to T_{crit}, the activation state of Rubisco decreased with heat treatment (Figure 2d). Importantly, a decline in Rubisco activation was observed from the beginning to the end of the experiment as leaves aged. This decline was observed earlier in heat-treated plants (day 3) compared to control plants (day 5), indicating that heat stress accelerated this decline in Rubisco function. Rubisco activation state, defined as the ratio of initial to total Rubisco activity, reflects the enzyme's operational efficiency under different conditions. Initial activity represents the enzyme's immediate functionality upon extraction, while total activity reflects its potential after full carbamylation (Ashton *et al.*, 2024). Although Rubisco activation state was similar on day 5, the initial and total activity was significantly lower in heat-treated

617 compared to control plants ($p < 0.001$, Figure 2d). This decrease in Rubisco activity on day
618 5 of the heatwave was associated with decreased Rubisco amount and TSP (Figure 2d), as
619 no significant differences were detected in Rubisco specific activity, expressed per quantity
620 of Rubisco protein (Supporting Information Fig. S8).

621 Heat stress induces the expression of thermotolerant Rca isoforms

622 Potential heat-induced changes in gene expression of *Rca* isoforms were assessed through
623 RNA sequencing analysis (RNA-seq) on days 1, 3 and 5 of the heatwave. A principal
624 component analysis (PCA) distinguished gene expression changes caused by heat stress
625 and those resulting from leaf aging (Figure 3a, Supporting Information Fig. S9). Heat-
626 induced differential gene expression occurred from the first day of the heatwave, with both
627 up and down-regulation of genes evident in heat-treated plants compared to control
628 conditions throughout the duration of the heatwave (Supporting Information Fig. S9). Heat
629 stress was confirmed by upregulation of the heat shock protein *HSP20* (Song *et al.*, 2017)
630 from day 1 of the heatwave (Figure 3b). The heatwave also decreased expression of the
631 Rubisco small subunit (*RbcS*), which is likely associated with the lower Rubisco amounts
632 (Figure 3c).

633 Under control temperature conditions, *Rca1β* was found to be the most abundant Rca
634 transcript, followed by *Rca8α*, while *Rca10α* and *Rca10β* were expressed at much lower
635 levels (Figure 3c). Of the hundreds of up and downregulated genes (Supporting Information
636 Fig. S9), volcano plots showed that *HSP20* and *Rca10* were both upregulated on days 1, 3,
637 and 5 of the heatwave (Supporting Information Fig. S10). Heat-treated plants showed a
638 (non-significant) tendency for lower *Rca1β* expression, whereas *Rca8α*, *Rca10α* and
639 *Rca10β* were all upregulated during the heatwave (Figure 3c). It is noteworthy that despite
640 the upregulation of both *Rca10* transcripts, their expression levels remained much lower
641 than *Rca1β* and *Rca8α* (Figure 3c). Changes in *HSP20* and the four *Rca* transcript levels
642 were also confirmed via RT-qPCR (Supporting Information Fig. S11). Moreover, promoter
643 analysis revealed multiple stress responsive elements in *Rca1β and Rca8α*, while *Rca10*
644 contains two heat stress response elements and has fewer other stress responsive elements
645 (Supporting Information Fig. S12).

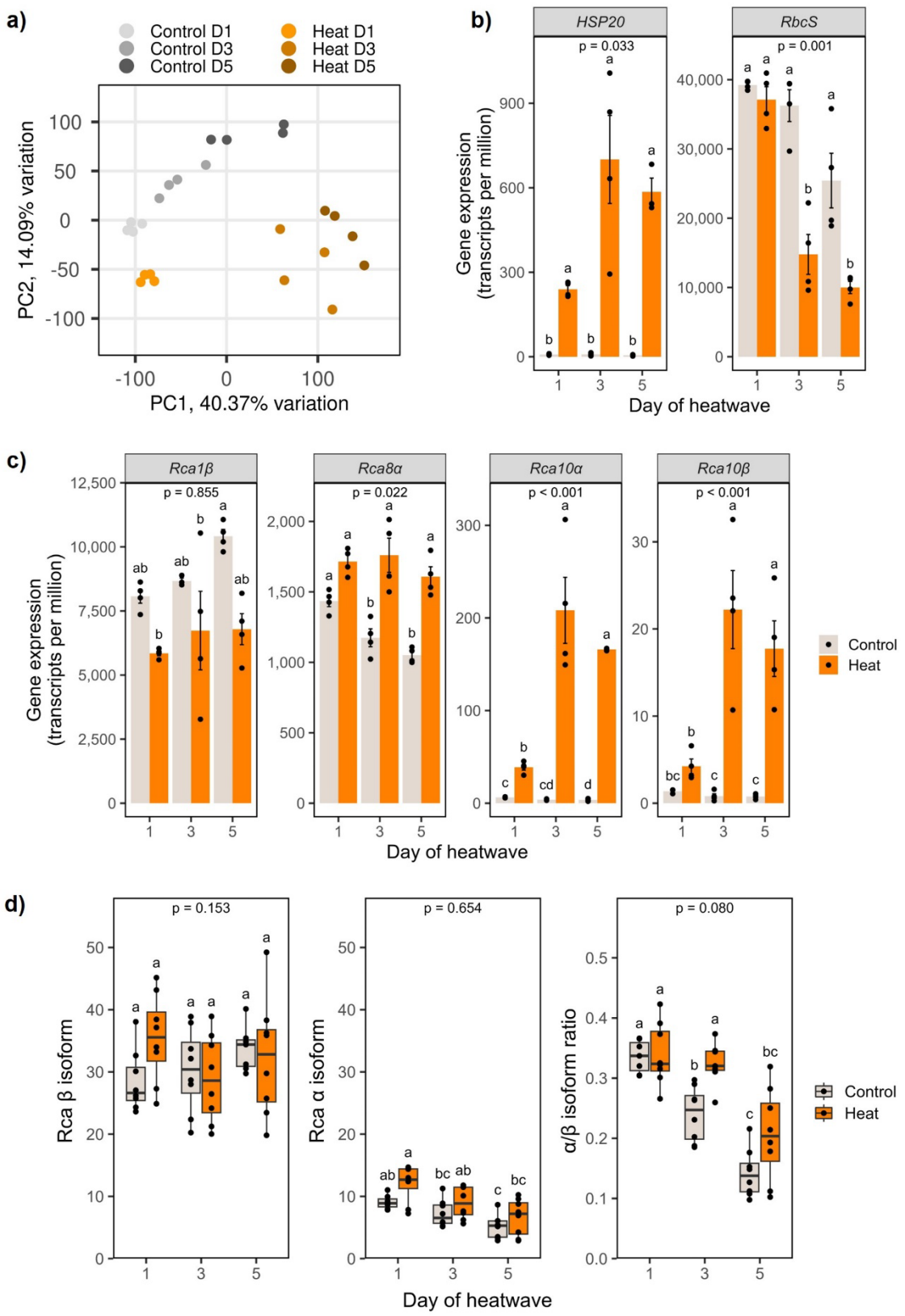

Figure 3. Differential gene expression and Rca protein abundance in cowpea during a heatwave. a) Principal components (PCA) plot of gene expression in leaves of heat-treated and control cowpea plants on days 1, 3 and 5 of the heatwave. b) Expression levels of the

650 heat shock protein 20 (HSP20) and the small Rubisco subunits (RbcS) were used as
651 reference. Bar plots represent means and error bars standard error. c) Expression levels of
652 the four cowpea Rca isoforms in control and heat-treated plant on days 1, 3 and 5 of the
653 heatwave (n=4). d) Protein abundance of Rca isoforms in leaves of control and heat-treated
654 plants on days 1, 3 and 5 of the heatwave (relative units). Rca α and β isoforms were
655 detected using an anti-Rca antibody and normalised to total protein. The size difference
656 between the α (45 kDa) and β (41 kDa) isoforms enabled the identification as separate
657 bands, and the estimation of the α/β ratio. P-values were calculated using two-way ANOVA
658 followed by Tukey post-hoc tests. Samples were run in separate gels and normalised to total
659 protein via reversible staining of the membrane. Blot images and full sample data are
660 provided in the source data file.

661

662 To investigate if changes in gene expression are reflected at protein level, the abundance of
663 leaf Rca protein was quantified via immunoblotting (Figure 3d). A pan-Rca antibody that
664 reacts with all isoforms of Rca and enables quantification of Rca α and Rca β isoforms, as
665 these run separately in gel electrophoresis due to the difference in molecular weight, was
666 used to identify changes in abundance between α and β isoforms (Perdomo *et al.*, 2018).
667 Whilst differential gene expression was observed, changes in Rca protein were less
668 pronounced. As *Rca10β* transcript levels are almost negligible compared to *Rca1β*, it is
669 reasonable to infer that the β isoform protein is predominantly attributable to *Rca1β*
670 expression. Expression of *Rca8α* is also likely to produce most of the α isoform protein. Rca
671 β remained unchanged during the heatwave, while the α isoform decreased from day 1 to
672 day 5 but was not significantly different between control and heat-treated plants (Figure 3d).
673 Protein abundance of Rca8α was also determined using a specific antibody that only reacts
674 with this isoform (Bloemers & Carmo-Silva, 2024). Rca8α showed a near identical pattern to
675 the pan-Rca antibody for Rca α with a non-significant tendency for increased abundance in
676 heat treated plants compared to the control (Supporting Information Fig. S13a). A significant
677 increase in the α/β ratio was however detected in day 3 of the heatwave, which may indicate
678 differences in the relative abundance of Rca isoforms (Figure 3d). Due to their very low
679 abundance, Rca10α & Rca10β protein isoforms were undetected in leaf extracts with Rca10
680 specific antibodies (Supporting Information Fig. S13b).

681 Heat-treated plants maintain Rca rate and thermal optimum

682 To test the hypothesis that heat-induced changes in the relative abundance of Rca isoforms
683 are reflected in activity, we characterised the temperature response of Rubisco reactivation
684 by Rca in protein extracts from leaves sampled on day 5 of the heatwave (Figure 4). Leaf

extracts were desalted to produce the free Rubisco apoenzyme (uncarbamylated form), which was subsequently inhibited through incubation with RuBP (Carmo-Silva & Salvucci, 2011). The inhibited Rubisco in the leaf extract was then used to determine the rate of reactivation by the Rca holoenzyme via removal of RuBP from uncarbamylated Rubisco catalytic sites, at a range of temperatures (Supporting Information Fig. S14). Concurrent measurement of spontaneous reactivation of Rubisco in the absence of ATP, which is required for Rca activity, enabled calculation of the spontaneous (Supporting Information Fig. S15) and Rca-mediated rate of Rubisco reactivation (Figure 4).

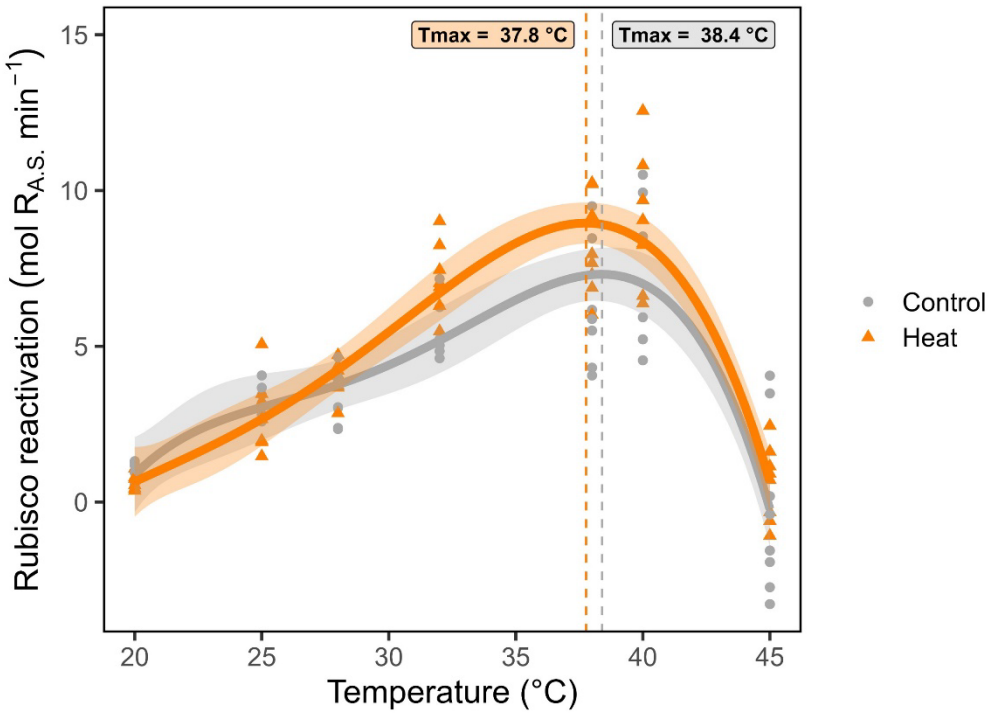

Figure 4. Temperature response of Rca activity in leaf extracts of control and heat-treated cowpea plants. Leaf discs were sampled on day 5 of the heatwave. The Rubisco and Rca contained in the leaves of each plant were extracted, Rubisco was inhibited by binding of RuBP to decarbamylated catalytic sites in the absence of CO_2 and Mg^{2+}, then reactivation by Rca was measured at varying temperatures by comparing an assay in presence of ATP and ATP-regenerating system with the negative control assay in the absence of ATP. The rate of Rubisco reactivation was calculated from measurements of Rubisco activity at 30 and 90 s after the start of the assay and expressed relative to maximum Rubisco activity in the same leaf extracts (as described in Supporting Information Fig. S14). Symbols represent biological replicates (leaf extracts from independent plant samples; n=8). Lines represent the best fit for each group of plants (selected by the Akaike information criterion) and coloured areas denote the 95% confidence interval for each fit (Supporting Information Table S9). Full sample data are provided in the source data file.

707

708 Rubisco reactivation by Rca tended to be faster in heat-treated compared to control plants,
709 however this increase was not statistically significant ($p > 0.05$, Figure 4). Heat-treated plants
710 exhibited similar thermal optima of Rubisco reactivation by Rca to control plants at
711 approximately 38 °C (Figure 4). T_{opt} and $T_{0.5}$ were also similar between control and heat-
712 treated plants (Table 2), indicating that the large fold-change in *Rca10* transcript abundance
713 (Figure 3c) and the small change in heat-induced protein Rca isoform ratio (Figure 3d) did
714 not alter the temperature profile of Rubisco reactivation by Rca in the leaves of heat-treated
715 plants (Figure 4). Interestingly, the T_{max}, T_{opt} and, to a lesser extent, $T_{0.5}$ of Rubisco
716 reactivation by Rca were higher in leaf extracts (Table 2) than the respective values
717 measured for each individual Rca isoform purified after recombinant expression (Table 1).

718

719 **Table 2. Temperature response of Rubisco activase (Rca) activity in leaf extracts.**
720 Maximum rate of Rubisco activation and corresponding temperature (T_{max}), optimum
721 temperature range (T_{opt}, above 70% activity) and temperature above the optimum at which
722 50% of the maximum activity remains ($T_{0.5}$). Values were estimated from best-fit models that
723 describe the temperature response of the pool of Rca isoforms extracted from leaves of control
724 and heat-treated cowpea on day 5 of the heatwave (Supporting Information Table S9). The
725 best-fit model for each treatment was applied to combined replicates shown in Figure 4 (n=6-
726 8).

Treatment	Rubisco reactivation$_{max}$ (mol $R_{A.S.}$ min^{-1})	T_{max} (°C)	T_{opt} (°C)	$T_{0.5}$ (°C)
Control	7.3	38.4	31.9 – 42.3	43.1
Heat	9.0	37.8	28.2 – 42.2	43.3

727

728 # Discussion

729 ## Cowpea Rca isoforms differ in thermal optima

730 We investigated the temperature response of Rubisco activase in cowpea, a vital crop for
731 sub-Saharan Africa that is adapted to warm temperatures, yet susceptible to the increasing
732 pressures of global warming. Several studies demonstrated that Rca thermolability limits
733 photosynthesis at elevated temperatures (Feller *et al.*, 1998; Crafts-Brandner & Law, 2000;
734 Salvucci *et al.*, 2006; Perdomo *et al.*, 2017), making it a target for enhancing crop yield
735 under elevated temperatures. In this study, we identified and characterised four Rca
736 isoforms in cowpea: Rca1β, Rca8α, Rca10α and Rca10β. *In vitro* analysis across a range of
737 temperatures revealed a higher thermal optimum for Rca10α and Rca10β for both ATPase
738 and Rubisco reactivation activities (Figure 1b). The most abundant Rca1β and Rca8α
739 isoforms in cowpea leaves (Figure 3) both exhibited lower thermal optima and thermal
740 maxima, as well as slower rates of catalysis for both activities compared to the isoforms
741 encoded by *Rca10* (Table 1).

742 Differences in thermal optima among isoforms have been reported for other species. In rice,
743 the α isoform is more thermotolerant while in wheat one of the two β isoforms exhibits a
744 higher thermal optima (Scafaro *et al.*, 2018; Shivhare *et al.*, 2019; Degen *et al.*, 2020). For
745 spinach, the β isoform is more sensitive to heat stress, with Rca β homo-hexamers
746 displaying a lower thermal midpoint compared to Rca α homo-hexamers or hetero-hexamers
747 comprising both α and β isoforms (Keown & Pearce, 2014). Notably, for all Rca isoforms, the
748 T_{max} for ATPase activity is higher than for Rubisco reactivation, potentially due to differential
749 oligomeric requirements for each activity. The proposed mechanism for Rca-mediated
750 Rubisco reactivation involves threading Rubisco through the AAA+ pore, akin to the method
751 employed by AAA+ ATPases that adjust the conformation of misfolded proteins (Bhat *et al.*,
752 2017; Houry *et al.*, 2017; Waheeda *et al.*, 2023). This mechanism requires hexameric Rca
753 for Rubisco reactivation, whilst ATP hydrolysis can occur with three Rca subunits forming an
754 oligomer (Keown *et al.*, 2013; Hazra *et al.*, 2015).

755 The maximum rates of both ATP hydrolysis and Rubisco reactivation were higher for the
756 Rca10 isoforms compared to Rca1β and Rca8α (Table 1). Similar differences among Rca
757 isoforms were observed in rice and wheat but only for ATP hydrolysis, with the more
758 thermostable Rca isoforms exhibiting lower Rubisco reactivation maxima compared to the
759 less thermostable isoforms (Scafaro *et al.*, 2016, 2019a; Shivhare & Mueller-Cajar, 2017;
760 Degen *et al.*, 2020). In cowpea, we show that the increased thermostability of Rca10
761 isoforms occurs without a penalty in Rubisco reactivation rate. The broader T_{opt} of Rca10α
762 and Rca10β spans and extends above the T_{opt} of Rca1β and Rca8α (Table 1). Thus,

763 Rca10α and Rca10β appear to be ideal candidates to maintain CO_2 assimilation by Rubisco
764 both at optimal and supra-optimal temperatures. Curiously, the promoter regions of both
765 Rca1β and Rca8α contain multiple stress responsive elements while Rca10α and Rca10β
766 have only two heat response elements (Supporting Information Fig. S12), suggesting an
767 engineering approach may be required to alter the Rca isoforms predominantly involved in
768 maintaining Rubisco activity *in planta.*

769 Cowpea responds dynamically to a 5-day 38/28 °C heatwave

770 A 5-day heatwave at the vegetative growth stage (10 °C increase to 38/28 °C day/night) is
771 considered moderate heat stress for most cowpea cultivars (Lonardi *et al.*, 2019; Barros *et*
772 *al.*, 2021). Plants were well-watered to avoid confounding effects of water deficit limiting the
773 diffusion of CO_2 to Rubisco sites (Carmo-Silva *et al.*, 2012). The leaf temperature only
774 increased to 32 °C (Figure 2a), plant growth parameters were only mildly impacted, and the
775 aboveground dry biomass remained unaffected (Figure 2bc). Notably, it has been shown that
776 a heatwave during the vegetative stage can have a delayed impact on cowpea yield
777 (Mohammed *et al.*, 2024), which would not necessarily be expressed as reduced biomass at
778 the end of the heatwave. T_{crit}, an indicator of thermal lability of PSII, was higher on day 5 of
779 the 38/28 °C heatwave (Figure 2c) suggesting some capacity for PSII thermal acclimation
780 (Perez & Feeley, 2020). In wheat, increased T_{crit} after exposure to elevated temperature in
781 field and controlled environment experiments correlated with a dynamic response of PSII to
782 heat stress (Posch *et al.*, 2022). On day 5 of the 38/28 °C heatwave, cowpea plants had
783 decreased Rubisco activities and amount, lower leaf thickness, total chlorophyll and TSP
784 (Figure 2b), suggesting accelerated leaf senescence. Similar results were observed in heat-
785 treated wheat (Qu *et al.*, 2023), which could have a delayed impact on biomass production.

786 Thermotolerant Rca isoforms increase but remain low under heat

787 At optimal temperatures, *Rca1β* was the isoform most abundantly expressed, with *Rca8α*
788 following, while *Rca10α* and *Rca10β* were only marginally expressed (Figure 3c). Under
789 heat stress, *Rca8α*, *Rca10α* and *Rca10β* expression was upregulated, however *Rca10*
790 transcript levels remained very low compared to *Rca1β* and *Rca8α*. The corresponding
791 protein abundance was only marginally higher for Rca8α and remained undetectable for
792 Rca10α and Rca10β (Supporting Information Fig. S13; Figure 3d). The Rca α/β ratio
793 decreased as the leaves aged, and on day 3 of the heatwave heat-treated plants maintained
794 higher α/β ratio than control pants (Figure 3d). Variation in Rca α/β ratio under optimal and
795 supra-optimal temperatures may reflect differences in thermostability and regulatory
796 mechanisms (Zhang & Portis, 1999; Wang *et al.*, 2010; Degen *et al.*, 2021). While Rca α is
797 subject to redox regulation via thioredoxin-f (Zhang & Portis, 1999; Shivhare *et al.*, 2019;

798 Kim *et al.*, 2020) and tends to be more sensitive to inhibition by ADP (Zhang & Portis, 1999;
799 Scafaro *et al.*, 2019b; Amaral *et al.*, 2024a), variation also exists in the properties of Rca β
800 isoforms (Scafaro *et al.*, 2019a; Perdomo *et al.*, 2019).

801 Changes in relative abundance of Rca isoforms under heat stress are species-specific
802 (Yamori & von Caemmerer, 2009). In *Arabidopsis*, the two isoforms are comparable in
803 thermotolerance and both increase with heat maintaining a 1:1 ratio (Ristic *et al.*, 2009).
804 Conversely, in rice and wheat, Rca isoforms differ in temperature response and heat induces
805 upregulation of the thermotolerant variants (Scafaro *et al.*, 2018, 2019a; Degen *et al.*, 2021).
806 While the same was observed for cowpea in the present study, the protein abundance of the
807 thermostable Rca isoforms remained below detection levels in plants exposed to the 5-day
808 38/28 °C heatwave. Overexpression of thermostable Rca via genetic engineering led to
809 enhanced photosynthesis and yield (Kurek *et al.*, 2007; Shivhare & Mueller-Cajar, 2017;
810 Scafaro *et al.*, 2018; Degen *et al.*, 2020). Increasing Rca thermostability, and to a lesser
811 extent upregulation of its quantity, have been shown to ameliorate the reduction in Rubisco
812 activation state caused by elevated temperatures (Kurek *et al.*, 2007; Scafaro *et al.*, 2018,
813 2019a; Kim *et al.*, 2020). The results presented here suggest that increasing Rca10α and
814 Rca10β abundance in cowpea, while possible in longer or hotter heat conditions, would
815 likely require an engineering approach.

816 Rubisco reactivation by Rca in cowpea remains unaltered under heat

817 The temperature response of Rubisco reactivation in leaf extracts of plants exposed to the 5-
818 day 38/28 °C heatwave showed a similar pattern and comparable thermal optima to control
819 plants (Figure 4). Scafaro *et al.* (2019a) reported increases Rubisco reactivation rate and $T_{0.5}$
820 of Rca in leaf extracts from heat-treated wheat. In cowpea, the minor increase in rate was
821 statistically insignificant and T_{opt} and $T_{0.5}$ were comparable between control and heat-treated
822 plants, with a slight increase of the T_{opt} range in heat-treated plants (Table 2). These results
823 indicate that the heatwave in the absence of water deficit caused only mild heat stress,
824 allowing plants to respond by adjusting isoform ratios in the leaf while preserving the Rca
825 rate and temperature response.

826 Interestingly, the T_{opt} upper bound determined in leaf extracts was 42 °C for control and
827 heat-treated plants, much higher than the T_{leaf} in heat-treated plants (Table 2, Figure 2a).
828 The maximum Rca rate in leaf extracts (Table 2) was also higher than the Rubisco
829 reactivation rate of each isoform measured *in vitro* (Table 1). Similar results were observed
830 in rice and wheat but only for the more thermostable isoforms (Scafaro *et al.*, 2016, 2019a).
831 Higher Rca rate in leaf extracts may be attributed to several possible factors: differences in
832 structural conformation of recombinant Rca, post-translational modifications that regulate

833 Rca activity in the leaf and are absent in recombinant proteins, hetero-hexamers comprising
834 different isoforms *in planta* exhibiting higher thermal optima, or interaction of Rca with other
835 components in the chloroplast. Chen *et al.* (2010) reported dynamic and reversible binding of
836 rice Rca to the thylakoid membrane while it is active in remodelling the conformation of
837 inhibitor-bound Rubisco. Binding of Rca to the thylakoid membrane has also been reported
838 during heat stress although its binding to the chloroplast ribosomes was proposed to have a
839 protective role (Rokka *et al.*, 2001). Moreover, heat stress has been shown to induce
840 association of Rca with β-subunit of chaperonin-60 (cpn60β), a potential heat shock
841 molecular chaperone (Salvucci, 2008). Thus, while *in vitro* analyses are useful to compare
842 the properties of the individual isoforms, *in vivo* analyses as shown here for cowpea enable
843 assessment of the overall Rca response within the chloroplast stroma.

844 Conclusion

845 Cowpea is a vital source of protein for sub-Saharan Africa, and depite being warm-adapted,
846 it is threatened by future heatwaves, which are likely to increase in intensity, duration, and
847 frequency. Here, we identified two isoforms of Rca that have higher thermal maxima,
848 broader thermal optima, and faster rates of ATP hydrolysis and Rubisco reactivation than the
849 predominant Rca isoforms present in cowpea leaves. We showed that a 5-day 38/28 °C
850 heatwave in the absence of water deficit caused leaf temperature to increase to 32 °C. Since
851 this temperature is below the temperature at which Rca activity decreased below 70% of
852 maximum for each Rca isoform, the impact of such a heatwave on Rubisco function and
853 biomass production was only mild. However, cowpea plants growing in smallholder farmer
854 fields in sub-Saharan Africa are likely to experience water deficit alongside warmer
855 heatwaves (Almazroui *et al.*, 2020; Song *et al.*, 2023). This combination can impact the
856 ability of the plant to cool its leaves leading to higher leaf temperatures (Carmo-Silva *et al.*,
857 2012; Fahad *et al.*, 2017; Sato *et al.*, 2024). Increasing the abundance of the superior
858 Rca10α and Rca10β isoforms characterised here provides an exciting opportunity to
859 enhance the resilience of cowpea and other crops to future extreme climates.

Acknowledgements:
We thank Dr Sam Taylor (Lancaster University) for input and discussions around experimental design and calculations for determining T_{crit}. Ben Davies (Lancaster University) supported plant maintenance, measurements and sampling. We thank Dr Rachel Baxter (Lancaster University) for assistance with data analysis, and Dr Joana Amaral for useful discussions on data interpretation.

Competing interests:
The authors declare no conflicts of interest.

Author contributions:
E.C.S conceived and supervised the research. A.G., R.P., I.R., D.J.O., E.C.S. designed experiments. M.T.P. designed and executed the cloning strategy. D.B., P.D.G., D.W. produced and purified recombinant proteins. D.W. and C.J.A. purified Rubisco. D.B. and A.G. performed ATP hydrolysis measurements. A.G. performed Rubisco reactivation measurements. R.P. and I.R. performed heatwave experiments. R.P. performed RNAseq, RT-qPCR and plant growth measurements. R.P. and P.D.G. performed promoter analyses. I.R. performed fluorescence measurements. A.G., R.P. and C.J.A. determined activity and amount of Rubisco and Rubisco activase in leaf extracts. A.G., R.P., C.J.A. and I.R. analysed the data. A.G. and E.C.S. wrote the manuscript with help from all authors.

Data availability:
Data presented are available in the accompanying supporting information and source data. The RNA-seq data reported in this article has been deposited in DDBJ's Sequence Read Archive (DRA) and are accessible through DRR BioProject accession number PRJDB19806. Processed RNA-seq data are submitted in the DDBJ's Genomic Expression Archive (GEA) and are accessible through the Experiment accession number (E-GEAD-889). Other data associated with the study are available from the corresponding author.

Funding:
This work was supported by the project Realizing Increased Photosynthetic Efficiency (RIPE), that is funded by Gates Agricultural Innovations grant investment 57248, awarded to Lancaster University by the University of Illinois, USA. D.B. was supported by a PhD scholarship from Lancaster University.

894 # References

895 **Akaike H**. **1974**. A new look at the statistical model identification. *IEEE Transactions on*
896 *Automatic Control* **19**: 716–723.

897 **Almazroui M, Saeed F, Saeed S, Nazrul Islam M, Ismail M, Klutse NAB, Siddiqui MH**.
898 **2020**. Projected change in temperature and precipitation over Africa from CMIP6. *Earth*
899 *Systems and Environment* **4**: 455–475.

900 **Amaral J, Lobo AKM, Carmo-Silva E**. **2024a**. Regulation of Rubisco activity in crops. *New*
901 *Phytologist* **241**: 35–51.

902 **Amaral J, Lobo AKM, Carmo-Silva E, Orr DJ**. **2024b**. Purification of Rubisco from Leaves.
903 In: Covshoff S, ed. Photosynthesis : Methods and Protocols. New York, NY: Springer US, 417–
904 426.

905 **Ara N, Nakkanong K, Lv W, Yang J, Hu Z, Zhang M**. **2013**. Antioxidant enzymatic activities
906 and gene expression associated with heat tolerance in the stems and roots of two Cucurbit
907 species ('*Cucurbita maxima*' and '*Cucurbita moschata*') and their interspecific inbred line
908 "*Maxchata*". *International Journal of Molecular Sciences* **14**: 24008.

909 **Ashton CJ, Page R, Lobo AKM, Amaral J, Siqueira JA, Orr DJ, Carmo-Silva E**. **2024**.
910 Radiometric determination of Rubisco activation state and quantity in leaves. In: Methods in
911 Enzymology. Academic Press.

912 **Bagati S, Rai GK, Bhadwal D, Berwal MK**. **2021**. Biotechnological approaches for the
913 development of heat stress tolerance in crop plants. In: Abiotic Stress Tolerance Mechanisms
914 in Plants. CRC Press.

915 **Barros JRA, Guimarães MJM, Silva RM e, Rêgo MTC, de Melo NF, de Melo Chaves AR,**
916 **Angelotti F**. **2021**. Selection of cowpea cultivars for high temperature tolerance: physiological,
917 biochemical and yield aspects. *Physiology and Molecular Biology of Plants* **27**: 29–38.

918 **Barta C, Carmo-Silva AE, Salvucci ME**. **2011**. Purification of Rubisco activase from leaves
919 or after expression in *Escherichia coli*. *Methods in Molecular Biology (Clifton, N.J.)* **684**: 363–
920 374.

921 **Becker R, Schüth C, Merz R, Khaliq T, Usman M, Beek T aus der, Kumar R, Schulz S**.
922 **2023**. Increased heat stress reduces future yields of three major crops in Pakistan's Punjab
923 region despite intensification of irrigation. *Agricultural Water Management* **281**: 108243.

924 **Bhat JY, Thieulin-Pardo G, Hartl FU, Wendler P, Mili Ci C G, Bracher A, Maxwell A,**
925 **Ciniawsky S, Mueller-Cajar O, Engen JR, *et al.* 2017**. Mechanism of enzyme repair by the
926 AAA + chaperone Rubisco activase. *Molecular Cell* **67**: 744–756.

927 **Blighe, K, S Rana, M Lewis**. **2018**. EnhancedVolcano: Publication-ready volcano plots with
928 enhanced colouring and labeling.

929 **Bloemers D, Carmo-Silva E**. **2024**. Antibody design for the quantification of photosynthetic
930 proteins and their isoforms. In: Covshoff S, ed. Photosynthesis : Methods and Protocols. New
931 York, NY: Springer US, 405–416.

932 **Bradford MM**. **1976**. A rapid and sensitive method for the quantitation of microgram quantities
933 of protein utilizing the principle of protein-dye binding. *Analytical Biochemistry* **72**: 248–254.

934 **Bretz F, Hothorn T, Westfall P**. **2016**. *Multiple Comparisons Using R*. CRC Press.

935 **Brown AV, Conners SI, Huang W, Wilkey AP, Grant D, Weeks NT, Cannon SB, Graham**
936 **MA, Nelson RT**. **2021**. A new decade and new data at SoyBase, the USDA-ARS soybean
937 genetics and genomics database. *Nucleic Acids Research* **49**: D1496–D1501.

938 **Carmo-Silva AE, Gore MA, Andrade-Sanchez P, French AN, Hunsaker DJ, Salvucci ME**.
939 **2012**. Decreased CO_2 availability and inactivation of Rubisco limit photosynthesis in cotton
940 plants under heat and drought stress in the field. *Environmental and Experimental Botany* **83**:
941 1–11.

942 **Carmo-Silva AE, Salvucci ME**. **2011**. The activity of Rubisco's molecular chaperone,
943 Rubisco activase, in leaf extracts. *Photosynthesis Research* **108**: 143–155.

944 **Carmo-Silva AE, Salvucci ME**. **2013**. The Regulatory Properties of Rubisco Activase Differ
945 among Species and Affect Photosynthetic Induction during Light Transitions 1. *Plant*
946 *Physiology Ȯ* **161**: 1645–1655.

947 **Carmo-Silva E, Scales JC, Madgwick PJ, Parry MAJ**. **2015**. Optimizing Rubisco and its
948 regulation for greater resource use efficiency. *Plant, Cell & Environment* **38**: 1817–1832.

949 **Chen H**. **2022**. VennDiagram: Generate High-Resolution Venn and Euler Plots.

950 **Chen J-H, Tang M, Jin X-Q, Li H, Chen L-S, Wang Q-L, Sun A-Z, Yi Y, Guo F-Q**. **2022**.
951 Regulation of Calvin–Benson cycle enzymes under high temperature stress. *aBIOTECH* **3**:
952 65.

953 **Chen J, Wang P, Mi H-L, Chen G-Y, Xu D-Q**. **2010**. Reversible association of ribulose-1, 5-
954 bisphosphate carboxylase/oxygenase activase with the thylakoid membrane depends upon
955 the ATP level and pH in rice without heat stress. *Journal of Experimental Botany* **61**: 2939–
956 2950.

957 **Chifflet S, Torriglia A, Chiesa R, Tolosa S**. **1988**. A method for the determination of inorganic
958 phosphate in the presence of labile organic phosphate and high concentrations of protein:
959 Application to lens ATPases. *Analytical Biochemistry* **168**: 1–4.

960 **Crafts-Brandner SJ, Law RD**. **2000**. Effect of heat stress on the inhibition and recovery of
961 the ribulose-1,5-bisphosphate carboxylase/oxygenase activation state. *Planta* **212**: 67–74.

962 **Crafts-Brandner SJ, Salvucci ME**. **2000**. Rubisco activase constrains the photosynthetic
963 potential of leaves at high temperature and CO_2. *Proceedings of the National Academy of*
964 *Sciences of the United States of America* **97**: 13430–13435.

965 **Degen GE, Orr DJ, Carmo-Silva E**. **2021**. Heat-induced changes in the abundance of wheat
966 Rubisco activase isoforms. *New Phytologist* **229**: 1298–1311.

967 **Degen GE, Worrall D, Carmo-Silva E**. **2020**. An isoleucine residue acts as a thermal and
968 regulatory switch in wheat Rubisco activase. *Plant Journal* **103**: 742–751.

969 **Fahad S, Bajwa AA, Nazir U, Anjum SA, Farooq A, Zohaib A, Sadia S, Nasim W, Adkins**
970 **S, Saud S, *et al.* 2017**. Crop production under drought and heat stress: Plant responses and
971 management options. *Frontiers in Plant Science* **8**.

Feller U, Crafts-Brandner SJ, Salvucci ME. **1998**. Moderately high temperatures inhibit ribulose-1,5-bisphosphate carboxylase/oxygenase (Rubisco) activase-mediated activation of Rubisco. *Plant Physiol* **116**: 539–546.

Galmés J, Hermida-Carrera C, Laanisto L, Niinemets Ü. **2016**. A compendium of temperature responses of Rubisco kinetic traits: variability among and within photosynthetic groups and impacts on photosynthesis modeling. *Journal of Experimental Botany* **67**: 5067–5091.

Gonçalves A, Goufo P, Barros A, Domínguez-Perles R, Trindade H, Rosa EAS, Ferreira L, Rodrigues M. **2016**. Cowpea (*Vigna unguiculata* L. Walp), a renewed multipurpose crop for a more sustainable agri-food system: nutritional advantages and constraints. *Journal of the Science of Food and Agriculture* **96**: 2941–2951.

Goodstein DM, Shu S, Howson R, Neupane R, Hayes RD, Fazo J, Mitros T, Dirks W, Hellsten U, Putnam N, *et al.* 2012. Phytozome: a comparative platform for green plant genomics. *Nucleic Acids Research* **40**: D1178–D1186.

Graves S, Piepho H-P, Selzer L, Dorai-Raj S. **2024**. multcompView: Visualizations of Paired Comparisons.

Harboure P. **2024**. WMO Global Annual to Decadal Climate Update.

Hatfield JL, Prueger JH. **2011**. Agroecology: Implications for Plant Response to Climate Change. In: Crop Adaptation to Climate Change. Wiley-Blackwell.

Hazra S, Henderson JN, Liles K, Hilton MT, Wachter RM. **2015**. Regulation of ribulose-1,5-bisphosphate carboxylase/oxygenase (Rubisco) activase. *The Journal of Biological Chemistry* **290**: 24222–24236.

Hermida-Carrera C, Kapralov MV, Galmés J. **2016**. Rubisco catalytic properties and temperature response in crops. *Plant Physiology* **171**: 2549.

Houry WA, Wachter R, Prahlad V, Hayer-Hartl M, Bhat JY, Thieulin-Pardo G, Hartl FU. **2017**. Rubisco activases: AAA+ chaperones adapted to enzyme repair. *Frontiers in Molecular Biosciences* **4**: 20.

Kassambara A. **2023**. ggpubr: 'ggplot2' Based Publication Ready Plots.

Keown JR, Griffin MDW, Mertens HDT, Pearce FG. **2013**. Small oligomers of ribulose-bisphosphate carboxylase/oxygenase (Rubisco) activase are required for biological activity. *The Journal of Biological Chemistry* **288**: 20607–20615.

Keown JR, Pearce FG. **2014**. Characterization of spinach ribulose-1,5-bisphosphate carboxylase/ oxygenase activase isoforms reveals hexameric assemblies with increased thermal stability. *Biochem. J* **464**: 413–423.

Kilian J, Whitehead D, Horak J, Wanke D, Weinl S, Batistic O, D'Angelo C, Bornberg-Bauer E, Kudla J, Harter K. **2007**. The AtGenExpress global stress expression data set: protocols, evaluation and model data analysis of UV-B light, drought and cold stress responses. *The Plant Journal* **50**: 347–363.

Kim SY, Stessman DJ, Wright DA, Spalding MH, Huber SC, Ort DR. **2020**. *Arabidopsis* plants expressing only the redox-regulated Rca-α isoform have constrained photosynthesis and plant growth. *Plant Journal* **103**: 2250–2262.

1013 **Kumar A, Li C, Portis AR**. **2009**. *Arabidopsis thaliana* expressing a thermostable chimeric
1014 Rubisco activase exhibits enhanced growth and higher rates of photosynthesis at moderately
1015 high temperatures. *Photosynthesis Research* **100**: 143–153.

1016 **Kurek I, Chang TK, Bertain SM, Madrigal A, Liu L, Lassner MW, Zhu G**. **2007**. Enhanced
1017 thermostability of *Arabidopsis* Rubisco activase improves photosynthesis and growth rates
1018 under moderate heat stress. *The Plant Cell* **19**: 3230–3241.

1019 **Law RD, Crafts-Brandner SJ**. **2001**. High temperature stress increases the expression of
1020 wheat leaf ribulose-1,5-bisphosphate carboxylase/oxygenase activase protein. *Archives of*
1021 *Biochemistry and Biophysics* **386**: 261–267.

1022 **Li G, Mao H, Ruan X, Xu Q, Gong Y, Zhang X, Zhao N**. **2002**. Association of heat-induced
1023 conformational change with activity loss of Rubisco. *Biochemical and Biophysical Research*
1024 *Communications* **290**: 1128–1132.

1025 **Liang Q, Muñoz-Amatriaín M, Shu S, Lo S, Wu X, Carlson JW, Davidson P, Goodstein**
1026 **DM, Phillips J, Janis NM, *et al.* 2024**. A view of the pan-genome of domesticated cowpea
1027 (*Vigna unguiculata* [L.] Walp.). *The Plant Genome* **17**: e20319.

1028 **Lichtenthaler HK**. **1987**. [34] Chlorophylls and carotenoids: Pigments of photosynthetic
1029 biomembranes. In: Plant Cell Membranes. Methods in Enzymology. Academic Press, 350–
1030 382.

1031 **Lin Pedersen T**. **2024**. patchwork: The Composer of Plots.

1032 **Lonardi S, la Mu~ Noz-Amatria In M, Liang Q, Shu S, Wanamaker SI, Lo S, Tanskanen**
1033 **J, Schulman AH, Zhu T, Luo M-C, *et al.* 2019**. The genome of cowpea (*Vigna unguiculata*
1034 [L.] Walp.). *The Plant Journal* **98**: 767–782.

1035 **Martin M**. **2011**. Cutadapt removes adapter sequences from high-throughput sequencing
1036 reads. *EMBnet.journal* **17**: 10.

1037 **Mathur S, Agrawal D, Jajoo A**. **2014**. Photosynthesis: Response to high temperature stress.
1038 *Journal of Photochemistry and Photobiology B: Biology* **137**: 116–126.

1039 **Mohammed SB, Ongom PO, Togola A, Boukar O**. **2024**. Enhancing Cowpea tolerance to
1040 elevated temperature: Achievements, challenges and future directions. *Agronomy* **14**: 513.

1041 **Moore CE, Meacham-Hensold K, Lemonnier P, Slattery RA, Benjamin C, Bernacchi CJ,**
1042 **Lawson T, Cavanagh AP**. **2021**. The effect of increasing temperature on crop photosynthesis:
1043 from enzymes to ecosystems. *Journal of Experimental Botany* **72**: 2822–2844.

1044 **Muggeo VMR**. **2017**. Interval estimation for the breakpoint in segmented regression: a
1045 smoothed score-based approach. *Australian & New Zealand Journal of Statistics* **59**: 311–
1046 322.

1047 **Murchie EH, Lawson T**. **2013**. Chlorophyll fluorescence analysis: a guide to good practice
1048 and understanding some new applications. *Journal of Experimental Botany* **64**: 3983–3998.

1049 **Nagarajan R, Gill KS**. **2018**. Evolution of Rubisco activase gene in plants. *Plant Molecular*
1050 *Biology* **96**: 69–87.

1051 **Orr DJ, Robijns AKJ, Baker CR, Niyogi KK, Carmo-Silva E**. **2023**. Dynamics of Rubisco
1052 regulation by sugar phosphate derivatives and their phosphatases. *Journal of Experimental*
1053 *Botany* **74**: 581–590.

1054 **Patro R, Duggal G, Love MI, Irizarry RA, Kingsford C**. **2017**. Salmon provides fast and bias-
1055 aware quantification of transcript expression. *Nature Methods* **14**: 417–419.

1056 **Perdomo JA, Buchner P, Carmo-Silva E**. **2021**. The relative abundance of wheat Rubisco
1057 activase isoforms is post-transcriptionally regulated. *Photosynthesis Research* **148**: 47–56.

1058 **Perdomo JA, Capó-Bauçà S, Carmo-Silva E, Galmés J**. **2017**. Rubisco and Rubisco
1059 activase play an important role in the biochemical limitations of photosynthesis in rice, wheat,
1060 and maize under high temperature and water deficit. *Frontiers in Plant Science* **8**: 490.

1061 **Perdomo JA, Degen GE, Worrall D, Carmo-Silva E**. **2019**. Rubisco activation by wheat
1062 Rubisco activase isoform 2β is insensitive to inhibition by ADP. *Biochemical Journal* **476**:
1063 2595–2606.

1064 **Perdomo JA, Sales CRG, Carmo-Silva E**. **2018**. Quantification of photosynthetic enzymes
1065 in leaf extracts by immunoblotting. *Methods in Molecular Biology (Clifton, N.J.)* **1770**: 215–
1066 227.

1067 **Perez TM, Feeley KJ**. **2020**. Photosynthetic heat tolerances and extreme leaf temperatures.
1068 *Functional Ecology* **34**: 2236–2245.

1069 **Portis AR**. **2003**. Rubisco activase - Rubisco's catalytic chaperone. *Photosynthesis Research*
1070 **75**: 11–27.

1071 **Portis AR, Li C, Wang D, Salvucci ME**. **2008**. Regulation of Rubisco activase and its
1072 interaction with Rubisco. *Journal of Experimental Botany* **59**: 1597–1604.

1073 **Posch BC, Hammer J, Atkin OK, Bramley H, Ruan Y-L, Trethowan R, Coast O**. **2022**.
1074 Wheat photosystem II heat tolerance responds dynamically to short- and long-term warming.
1075 *Journal of Experimental Botany* **73**: 3268–3282.

1076 **Qu L, Gu X, Li J, Guo J, Lu D**. **2023**. Leaf photosynthetic characteristics of waxy maize in
1077 response to different degrees of heat stress during grain filling. *BMC Plant Biology* **23**: 469.

1078 **Ristic Z, Momčilović I, Bukovnik U, Prasad PVV, Fu J, DeRidder BP, Elthon TE,**
1079 **Mladenov N**. **2009**. Rubisco activase and wheat productivity under heat-stress conditions.
1080 *Journal of Experimental Botany* **60**: 4003–4014.

1081 **Robinson SP, Portis AR**. **1989**. Adenosine triphosphate hydrolysis by purified Rubisco
1082 activase. *Archives of Biochemistry and Biophysics* **268**: 93–99.

1083 **Rokka A, Zhang L, Aro EM**. **2001**. Rubisco activase: An enzyme with a temperature-
1084 dependent dual function? *Plant Journal* **25**: 463–471.

1085 **Ruuska S, Andrews TJ, Badger MR, Hudson GS, Laisk A, Price GD, Caemmerer S von**.
1086 **1998**. The interplay between limiting processes in C3 photosynthesis studied by rapid-
1087 response gas exchange using transgenic tobacco impaired in photosynthesis. *Functional*
1088 *Plant Biology* **25**: 859–870.

1089 **Sales CRG, Molero G, Evans JR, Taylor SH, Joynson R, Furbank RT, Hall A, Carmo-**
1090 **Silva E**. **2022**. Phenotypic variation in photosynthetic traits in wheat grown under field versus
1091 glasshouse conditions. *Journal of Experimental Botany* **73**: 3221–3237.

1092 **Salvucci ME**. **2008**. Association of Rubisco activase with chaperonin-60b: a possible
1093 mechanism for protecting photosynthesis during heat stress. *Journal of Experimental Botany*
1094 **59**: 1923–1933.

1095 **Salvucci ME, Crafts-Brandner SJ**. **2004**. Relationship between the heat tolerance of
1096 photosynthesis and the thermal stability of Rubisco activase in plants from contrasting thermal
1097 environments. **134**: 1460–1470.

1098 **Salvucci ME, DeRidder BP, Portis AR**. **2006**. Effect of activase level and isoform on the
1099 thermotolerance of photosynthesis in Arabidopsis. *Journal of Experimental Botany* **57**: 3793–
1100 3799.

1101 **Salvucci ME, Osteryoung KW, Crafts-Brandner SJ, Vierling E**. **2001**. Exceptional
1102 Sensitivity of Rubisco Activase to Thermal Denaturation in Vitro and in Vivo. *Plant Physiology*
1103 **127**: 1053–1064.

1104 **Sato H, Mizoi J, Shinozaki K, Yamaguchi-Shinozaki K**. **2024**. Complex plant responses to
1105 drought and heat stress under climate change. *The Plant Journal* **117**: 1873–1892.

1106 **Scafaro AP, Atwell BJ, Muylaert S, Reusel BV, Ruiz GA, Rie JV, Gallé A**. **2018**. A
1107 thermotolerant variant of Rubisco activase from a wild relative improves growth and seed yield
1108 in rice under heat stress. *Frontiers in Plant Science* **9**: 1663.

1109 **Scafaro AP, Bautsoens N, den Boer B, Van Rie J, Gallé A**. **2019a**. A Conserved sequence
1110 from heat-adapted species improves Rubisco activase thermostability in wheat. *Plant*
1111 *Physiology* **181**: 43–54.

1112 **Scafaro AP, Gallé A, Van Rie J, Carmo-Silva E, Salvucci ME, Atwell BJ**. **2016**. Heat
1113 tolerance in a wild *Oryza* species is attributed to maintenance of Rubisco activation by a
1114 thermally stable Rubisco activase ortholog. *New Phytologist* **211**: 899–911.

1115 **Scafaro AP, Posch BC, Evans JR, Farquhar GD, Atkin OK**. **2023**. Rubisco deactivation and
1116 chloroplast electron transport rates co-limit photosynthesis above optimal leaf temperature in
1117 terrestrial plants. *Nature Communications* **14**: 2820.

1118 **Scafaro AP, Vleesschauwer DD, Bautsoens N, Hannah MA, Boer B den, Gallé A, Rie JV**.
1119 **2019b**. A single point mutation in the C-terminal extension of wheat Rubisco activase
1120 dramatically reduces ADP inhibition via enhanced ATP binding affinity. *The Journal of*
1121 *Biological Chemistry* **294**: 17931.

1122 **Serban AJ, Breen IL, Bui HQ, Levitus M, Rebekka Wachter XM, Jez JM**. **2018**. Assembly–
1123 disassembly is coupled to the ATPase cycle of tobacco Rubisco activase. *J. Biol. Chem* **293**:
1124 19451–19465.

1125 **Shivhare D, Mueller-Cajar O**. **2017**. *In vitro* characterization of thermostable CAM Rubisco
1126 activase reveals a Rubisco interacting surface loop. **174**: 1505–1516.

1127 **Shivhare D, Ng J, Tsai Y-CC, Mueller-Cajar O**. **2019**. Probing the rice Rubisco-Rubisco
1128 activase interaction via subunit heterooligomerization. *Proceedings of the National Academy*
1129 *of Sciences of the United States of America* **116**: 24041–24048.

Song J, Tong G, Chao J, Chung J, Zhang M, Lin W, Zhang T, Bentler PM, Zhu W. **2023**. Data driven pathway analysis and forecast of global warming and sea level rise. *Scientific Reports* **13**: 5536.

Song K, Yim WC, Lee B-M. **2017**. Expression of heat shock proteins by heat stress in soybean. *Plant Breeding and Biotechnology* **5**: 344–353.

Stainbrook SC, Aubuchon LN, Chen A, Johnson E, Si A, Walton L, Ahrendt AJ, Strenkert D, Jez JM. **2024**. C4 grasses employ distinct strategies to acclimate Rubisco activase to heat stress. *Bioscience Reports* **44**.

Stotz M, Mueller-Cajar O, Ciniawsky S, Wendler P, Hartl FU, Bracher A, Hayer-Hartl M. **2011**. Structure of green-type Rubisco activase from tobacco. *Nature Structural & Molecular Biology* **18**: 1366–1370.

Taylor SH, Gonzalez-Escobar E, Page R, Parry MAJ, Long SP, Carmo-Silva E. **2022**. Faster than expected Rubisco deactivation in shade reduces cowpea photosynthetic potential in variable light conditions. *Nature Plants* **8**: 118–124.

Taylor SH, Orr DJ, Carmo-Silva E, Long SP. **2020**. During photosynthetic induction, biochemical and stomatal limitations differ between Brassica crops. *Plant, Cell & Environment* **43**: 2623–2636.

Waheeda K, Kitchel H, Wang Q, Chiu P-L. **2023**. Molecular mechanism of Rubisco activase: Dynamic assembly and Rubisco remodeling. *Frontiers in Molecular Biosciences* **10**: 1125922.

Wang D, Li X-F, Zhou Z-J, Feng X-P, Yang W-J, Jiang D-A. **2010**. Two Rubisco activase isoforms may play different roles in photosynthetic heat acclimation in the rice plant. *Physiologia Plantarum* **139**: 55–67.

Warrag MOA, Hall AE. **1984**. Reproductive responses of cowpea (*Vigna unguiculata* (L.) Walp.) to heat stress. II. Responses to night air temperature. *Field Crops Research* **8**: 17–33.

Weber E, Engler C, Gruetzner R, Werner S, Marillonnet S. **2011**. A modular cloning system for standardized assembly of multigene constructs. *PLOS ONE* **6**: e16765.

Werner S, Engler C, Weber E, Gruetzner R, Marillonnet S. **2012**. Fast track assembly of multigene constructs using Golden Gate cloning and the MoClo system. *Bioengineered Bugs* **3**: 38–43.

Wickham H. **2017**. Tidyverse: Easily install and load the 'tidyverse'. *R package version* **1**: 2017.

Wijewardene I, Shen G, Zhang H. **2021**. Enhancing crop yield by using Rubisco activase to improve photosynthesis under elevated temperatures. **1**: 2.

Winter D, Vinegar B, Nahal H, Ammar R, Wilson GV, Provart NJ. **2007**. An "Electronic fluorescent pictograph" browser for exploring and analyzing large-scale biological data sets. *PLOS ONE* **2**: e718.

Wood SN. **2017**. *Generalized Additive Models: An Introduction with R, Second Edition*. New York: Chapman and Hall/CRC.

Yamori W, von Caemmerer S. **2009**. Effect of Rubisco activase deficiency on the temperature response of CO_2 assimilation rate and Rubisco activation state: Insights from

1170 transgenic tobacco with reduced amounts of Rubisco activase. *Plant Physiology* **151**: 2073–
1171 2082.

1172 **Yin Z, Zhang Z, Deng D, Chao M, Gao Q, Wang Y, Yang Z, Bian Y, Hao D, Xu C**. **2014**.
1173 Characterization of Rubisco activase genes in maize: An α-isoform gene functions alongside
1174 a β-isoform gene. *Plant Physiology* **164**: 2096–2106.

1175 **Zahra N, Hafeez MB, Wahid A, Al Masruri MH, Ullah A, Siddique KHM, Farooq M**. **2023**.
1176 Impact of climate change on wheat grain composition and quality. *Journal of the Science of*
1177 *Food and Agriculture* **103**: 2745–2751.

1178 **Zhang N, Kallis RP, Ewy RG, Portis AR**. **2002**. Light modulation of Rubisco in *Arabidopsis*
1179 requires a capacity for redox regulation of the larger Rubisco activase isoform. *Proceedings*
1180 *of the National Academy of Sciences of the United States of America* **99**: 3330–3334.

1181 **Zhang N, Portis AR**. **1999**. Mechanism of light regulation of Rubisco: A specific role for the
1182 larger Rubisco activase isoform involving reductive activation by thioredoxin-f. *Plant Biology*
1183 **96**: 9438–9443.

1184

1185 # Supporting Information

1186 **Supporting Information Figures**

1187 Fig. S1. Amino acid residue alignment of the four cowpea Rca isoforms.

1188 Fig. S2. *In vitro* Rubisco reactivation by the four cowpea Rca isoforms.

1189 Fig. S3. Heatwave experimental design and cabinet temperature monitoring.

1190 Fig. S4. Cabinet plant layout design.

1191 Fig. S5. Leaf temperature monitoring over the heatwave experiment.

1192 Fig. S6. Growth parameters and chlorophyll content during and after heat stress.

1193 Fig. S7. T_{crit} calculation from temperature response of chlorophyll fluorescence-derived Fv/Fm.

1194 Fig. S8. Specific Rubisco activities of control and heat-treated plants.

1195 Fig. S9. Differential gene expression in heat-treated *versus* control cowpea plants.

1196 Fig. S10. Volcano plots depicting differential gene expression based on log change across the
1197 days of heatwave.

1198 Fig. S11. Gene expression of heat shock protein 20 (HSP20) and cowpea Rca transcripts.

1199 Fig. S12. Potential cis-acting regulatory elements in cowpea Rca promoter regions.

1200 Fig. S13. Protein abundance of Rca isoforms in leaves of control and heat-treated plants.

1201 Fig. S14. Protocol outline for determination of Rca activity in leaf extracts (LE).

1202 Fig. S15. Rubisco reactivation by the pool of cowpea Rca isoforms in leaf extracts (LE).

1203 **Supporting Information Tables**

1204 Table S1. Reference protein sequences used to identify cowpea Rca genes.

1205 Table S2. Primer sequences for adding Golden Gate overhangs to Rca coding regions.

1206 Table S3. Optimum temperature of in vitro Rubisco activase (Rca) activity.

1207 Table S4. Modelling of the *in vitro* temperature response of ATP hydrolysis and Rubisco
1208 activation by cowpea Rca isoforms.

1209 Table S5. RNA sample QC analysis prior to RNA sequencing.

1210 Table S6. Sequencing and alignment statistics.

1211 Table S7. MIQE checklist for RT-qPCR.

1212 Table S8. RT-qPCR primers.

1213 Table S9. Modelling of the temperature response of Rubisco activation by cowpea Rca in leaf
1214 extracts of control and heat-treat plants.

1215 Table S10. Leaf total soluble protein (TSP) and chlorophyll content.

1216 References